Latin American Journal of Solids and Structures
www.lajss.org

Three-Dimensional Rail–Bridge Coupling Element of Unequal Lengths for Analyzing Train–Track–Bridge Interaction System

Abstract

A three-dimensional rail-bridge coupling element of unequal lengths in which the length of the rail element is shorter than that of the bridge element is presented in this paper to investigate the spatial dynamic responses of a train-track-bridge interaction system. Formulation of stiffness and damping matrices for the fastener, ballast, and bearing, as well as the three-dimensional equations of motion in matrix form for a train-track-bridge interaction system using the proposed element are derived in detail using the energy principle. The accuracy of the proposed three-dimensional rail-bridge coupling element is verified using the existing two-dimensional element. Three examples of a seven-span continuous beam bridge are shown: the first investigates the influence of the efficiency and accuracy of the lengths of the rail and bridge elements on the spatial dynamic responses of the train-track-bridge interaction system, and the other two illustrate the influence of two types of track models and two types of wheel-rail interaction models on the dynamic responses of the system. Results show that (1) the proposed rail-bridge coupling element is not only able to help conserve calculation time, but it also gives satisfactory results when investigating the spatial dynamic responses of a train-track-bridge interaction system; (2) the double-layer track model is more accurate in comparison with the single-layer track model, particularly in relation to vibrations of bridge and rail; and (3) the no-jump wheel-rail interaction model is generally reliable and efficient in predicting the dynamic responses of a train-track-bridge interaction system.

Keywords

Three-dimensional rail-bridge, coupling element, unequal length, bridge, track, finite element method

Zhi-Ping Zeng [a]
Fu-Shan Liu [a,*]
Zhao-Hui Lu [a]
Zhi-Wu Yu [a]
Ping Lou [a]
Ling-Kun Chen [b]

[a] School of Civil Engineering, Central South University, Changsha 410075, China.
[b] College of Civil Science and Engineering, Yangzhou University, Yangzhou 225127, China.

Corresponding author:
[*] fushan0716@qq.com (Fu-Shan Liu)

http://dx.doi.org/10.1590/1679-78252551

Received 18.10.2015
In revised form 01.06.2016
Accepted 07.07.2016
Available online 03.08.2016

1 INTRODUCTION

A considerable amount of research has been conducted on the dynamic responses of railway bridge/track structures subjected to a moving train (Sun and Dhanasekar, 2002; Liu et al., 2009; Lu et al., 2009; Wang et al., 2010; Kim, 2011; Zakeri et al., 2014; Lei and Wang, 2014; Xu et al., 2015). Such research has been conducted particularly in the past three decades and mostly in relation to the rapid development of high-speed railways worldwide. However, due to the massive volume of work conducted, it is difficult to have a complete count of the number of studies and it is only possible to cite a few of those that are most relevant here.

The dynamic response of structures in relation to moving vehicles has been studied by previous researchers by modeling a moving vehicle as a moving load, moving mass, or a moving sprung mass with consideration of suspension (Ayre et al., 1950; Frýba, 1972; Chu et al., 1979; Wu and Dai, 1987; Chatterjee et al., 1994; Ichikawa et al., 2000). More sophisticated models that also consider the vertical dynamic interaction between the moving train and structures have also been implemented by a large number of researchers in recent years. For example, Zhai and Sun (1994) developed a new and detailed model to investigate the vertical interaction between a vehicle and the track in which the vehicle was modeled as a multi-body system with 10 degrees of freedom (DOFs), the track as an infinite Euler beam, and the wheel–rail interaction as a Hertzian nonlinear contact spring. In addition, Yang et al. (1999) derived a vehicle–bridge interaction element by considering a vehicle as a rigid beam supported by two suspension units and a bridge as beam elements, and Cheng et al. (2001) proposed a bridge-track-vehicle element in which the vehicles were modeled as mass-spring-damper systems, the rails as an upper beam element, and the bridge deck as a lower beam element. Furthermore, Lei and Noda (2002) developed a dynamic computational model for a vehicle and track coupling system using the finite element method (FEM), in which the vehicle-track coupling dynamic responses were analyzed in time and frequency domains due to the random irregularity of the track vertical profile. Thereafter, Wu and Yang (2003) investigated the vertical dynamic responses of a vehicle-rails-bridge interaction system using a condensation technique, which included the steady-state response and riding comfort of the train as well as the impact response of the rails and bridges. Based on the principle of a stationary value of total potential energy of dynamic system, Zeng (2003), Lou (2005), and Lou and Zeng (2005) derived equations of motion in a matrix form for three types of vehicle-track-bridge vertical interaction elements, in which the rails and the bridge deck were represented by an elastic Bernoulli-Euler upper beam with finite length and a simply supported Bernoulli-Euler lower beam, respectively. A later study by Lou (2007) investigated the vertical dynamic responses of a train-track-bridge interaction (TTBI) system using FEM, and by discretizing the slab track subsystem into track elements that flow with the moving vehicle, Lei and Wang (2014) developed a new approach with finite elements in a moving frame of reference to investigate the dynamic behavior of the train and slab track coupling system.

In addition, with the exception of work that has been restricted to mainly analyzing the two-dimensional (2D) dynamic responses of a train-track/bridge interaction system, a great volume of research has also dealt with three-dimensional (3D) aspects of the system. For example, Zhai et al. (1996) presented a new vertical and lateral coupling model of vehicle-track interaction, and investigated the safety limits against derailment due to track twist and the combined alignment and cross-level irregularities. In addition, Xia et al. (2000) studied the dynamic responses of the bridge-train

system, and the derailment and the offload factors related to the running safety of the train, using a 3D finite element model to represent the bridge. Furthermore, Wu et al. (2001) developed a vehicle-rail-bridge interaction model to analyze the 3D dynamic interaction between moving trains and the railway bridge, and Dinh et al. (2009) developed a formulation for 3D dynamic interactions between a bridge and a high-speed train using wheel-rail interfaces, where the bridge eccentricities and deck displacement due to torsion were accounted for in bridge deck modeling. Papers have also been written addressing the dynamic interaction between the track/bridge and the moving train, and some monographs have focused on this subject. For example, Song et al. (2003), Kwasniewski et al. (2006), Nguyen et al. (2009), Lei and Zhang (2011), Xin and Gao (2011), and Zhai et al. (2013) proposed a theory and method for dealing with the dynamic problem of the vehicle-track/bridge interaction system, respectively.

In the aforementioned works, most researchers have established the track-bridge interaction model using FEM, in which a rail-bridge coupling element of equal lengths (i.e., with the length of the rail element equal to that of the bridge element) is adopted. When the length of the bridge increases, the DOFs of the track-bridge interaction system also increase, and thus making a dynamic analysis of a track-bridge interaction system is a relatively time consuming process when using a rail-bridge coupling element of equal lengths. Therefore, the aim of this paper is to present a 3D rail-bridge coupling element of unequal lengths, in which sleepers are considered and where the length of the bridge element is longer than that of the rail element, to investigate the spatial dynamic responses of a TTBI system under the action of track irregularities. This paper can therefore be regarded as an extension of the theory presented by Lou et al. (2012), in which a 2D (vertical) rail-bridge coupling element of unequal lengths was proposed to analyze the vertical dynamic responses of a TTBI system. However, the possibility of considering the lateral responses of a TTBI system in the current work allows for a more realistic analyses.

In this study, a seven-span continuous beam bridge is used as an example, the influences of the lengths of the bridge and rail elements, two types of track models, and two types of wheel-rail interaction models on the efficiency and accuracy for calculating the spatial dynamic responses of the TTBI system excited by track irregularities are carried out, based on which some conclusions are drawn.

2 A 3D RAIL-BRIDGE COUPLING ELEMENT OF UNEQUAL LENGTHS

2.1 Model

A typical 3D rail-bridge coupling element of unequal lengths is shown in Figure 1 in which the length of the rail element is shorter than that of the bridge element (the corresponding physical parameters in Figure 1 are defined in Table 1). In the present study, the spatial dynamic behavior is studied while the axial deformations of the rail and bridge are ignored. Using a case of a double-track bridge, the dynamic responses of only one track is investigated and the other track is considered to be the dead load of the bridge, because the flexural rigidity of the bridge is usually thousands of times greater than that of the rails (or even tens of thousands). The proposed 3D coupling element ultimately consists of several rail elements of equal lengths (including the left and right rail), a bridge element, a few sleepers, a series of fasteners, and a series of discrete ballasts. It can

also include a bearing that connects a pier node at a supporting point of the bridge. The rails, bridges, and piers are modeled as uniform Bernoulli-Euler beams, while each sleeper is modeled as a rigid body, and the lateral and vertical elasticity and damping properties of the fastener, ballast, and bearing are modeled using discrete massless springs and dampers. The mass of the ballast is also added to the dead load of the bridge. As the longitudinal vibrations are neglected, each node in the rail and bridge elements has five DOFs, i.e., a lateral displacement along the y-axis, a vertical displacement along the z-axis, and three rotations about the x-, y-, and z-axes. Each sleeper and each node in the pier element has three DOFs, i.e., a lateral displacement along the y-axis, a vertical displacement along the z-axis, and a rotation about the x-axis. The positive directions of these DOFs accord with those of the co-ordinate, as shown in Figure 1. In addition, it is assumed that the length of the bridge element (LBE) is an integer number of times of the length of the rail element (LRE).

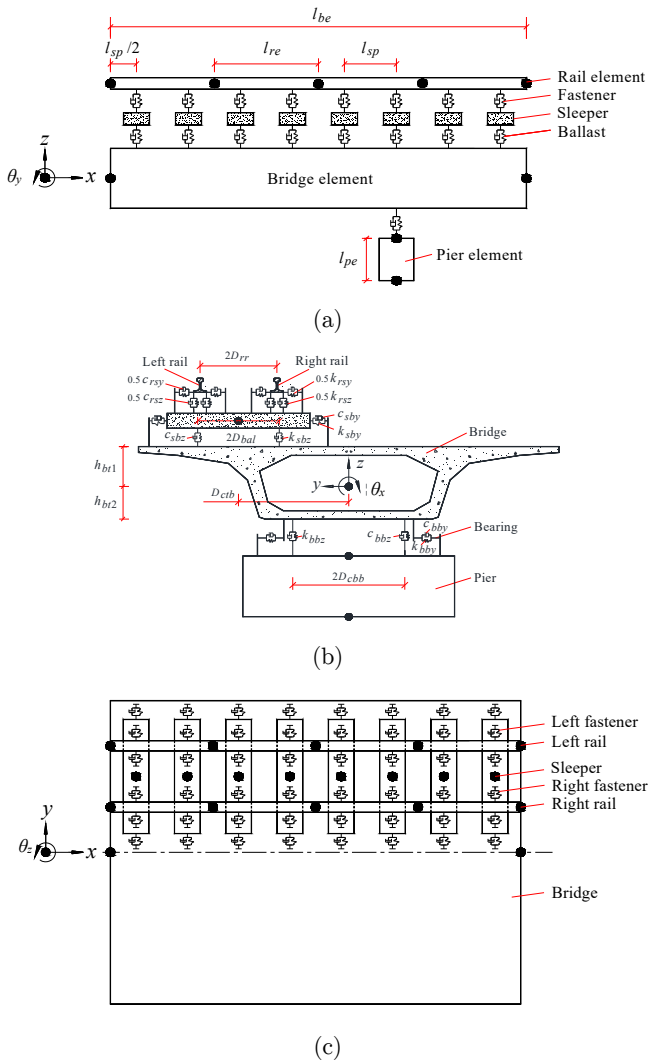

Figure 1: Typical 3D rail–bridge coupling element of unequal lengths: (a) frontal view, (b) left side view, and (c) top view.

Track		
Notation	Parameter	Value
A_r (m^2)	Sectional area of rail	77.45E-4
E_r (N/m^2)	Young's modulus of rail	2.10E11
G_r (N/m^2)	Shear modulus of rail	8.08E-10
$\bar{m}_r$ (kg/m)	Mass per unit length of rail	60.64
h_{rt1} (m)	Vertical distance between rail top and its center of torsion	94.53E-3
h_{rt2} (m)	Vertical distance between rail bottom and its center of torsion	81.47E-3
b_{rt} (m)	Half of width of rail bottom	75.00E-3
l_{re} (m)	Length of rail element (LRE)	-
I_{rx} (m^4)	Torsional moment of inertia about x-axis of rail	2.43E-5
I_{ry} (m^4)	Flexural moment of inertia about y-axis of rail	3.22E-5
I_{rz} (m^4)	Flexural moment of inertia about z-axis of rail	5.24E-6
m_s (kg)	Mass of a sleeper	340
J_{sx} ($kg \cdot m^2$)	Moment of inertia about x-axis of sleeper	74.2
l_{sp} (m)	Sleeper space	0.625
D_{rr} (m)	Half of transverse distance between center lines of two rails	0.75
D_{bal} (m)	Half of transverse distance between the two supporting points of ballast	0.75
k_{rsy} (N/m)	Lateral stiffness of discrete spring reflecting the property of fastener	3.0E7
k_{rsz} (N/m)	Vertical stiffness of discrete spring reflecting the property of fastener	6.0E7
c_{rsy} (N·s/m)	Lateral damping coefficient of discrete damper reflecting the property of fastener	5.0E4
c_{rsz} (N·s/m)	Vertical damping coefficient of discrete damper reflecting the property of fastener	7.5E4
k_{sby} (N/m)	Lateral stiffness of discrete spring reflecting the property of ballast under single rail	5.0E7
k_{sbz} (N/m)	Vertical stiffness of discrete spring reflecting the property of ballast under single rail	2.25E8
c_{sby} (N·s/m)	Lateral damping coefficient of discrete damper reflecting the property of ballast under single rail	4.0E4
c_{sbz} (N·s/m)	Vertical damping coefficient of discrete damper reflecting the property of ballast under single rail	6.0E4
Bridge		
Notation	Parameter	Value
A_b (m^2)	Sectional area of bridge	12.83
E_b (N/m^2)	Young's modulus of bridge	3.45E10
G_b (N/m^2)	Shear modulus of bridge	1.44E10
$\bar{m}_b$ (kg/m)	Mass per unit length of bridge	4.38E10
h_{bt1} (m)	Vertical distance between bridge deck and its center of torsion	1.42
h_{bt2} (m)	Vertical distance between bridge bottom and its center of torsion	1.88
D_{ctb} (m)	Half of transverse distance between center lines of two tracks	2.5
D_{cbb} (m)	Half of transverse distance between center lines of bearing	2.4
l_{be} (m)	Length of bridge element (LBE)	-
I_{bx} (m^4)	Torsional moment of inertia about x-axis of bridge	51.9
I_{by} (m^4)	Flexural moment of inertia about y-axis of bridge	19.2
I_{bz} (m^4)	Flexural moment of inertia about z-axis of bridge	134.0
k_{bby} (N/m)	Half of lateral stiffness of discrete spring reflecting the property of bearing	2.5E8
k_{bbz} (N/m)	Half of vertical stiffness of discrete spring reflecting the property of bearing	3.0E9

c_{bby} (N·s/m)	Half of lateral damping coefficient of discrete damper reflecting the property of bearing	1.0E5
c_{bbz} (N·s/m)	Half of vertical damping coefficient of discrete damper reflecting the property of bearing	1.0E6
ζ_b	Damping ratio of bridge	0.05
	Pier	
Notation	Parameter	Value
A_p (m^2)	Sectional area of pier	22.07
E_p (N/m^2)	Young's modulus of pier	3.15E10
$\bar{m}_p$(kg/m)	Mass per unit length of pier	5.51E4
l_{pe} (m)	Length of pier element (LPE)	-
I_{px} (m^4)	Flexural moment of inertia about x-axis of pier	101.9
k_{bby} (N/m)	Half of lateral stiffness of discrete spring reflecting the property of bearing	2.5E8
k_{bbz} (N/m)	Half of vertical stiffness of discrete spring reflecting the property of bearing	3.0E9
c_{bby} (N·s/m)	Half of lateral damping coefficient of discrete damper reflecting the property of bearing	1.0E5
c_{bbz} (N·s/m)	Half of vertical damping coefficient of discrete damper reflecting the property of bearing	1.0E6
ζ_p	Damping ratio of pier	0.05

Table 1: Major parameters of track and bridge.

2.2 Formulation of Stiffness and Damping Matrices of Fastener

For both the vertical and lateral discrete springs and dampers representing a fastener, one end point connects with an element of the left or right rail, while the other end point connects with a sleeper, as shown in Figures 1 and 2. Taking as an example the vertical discrete spring modeling with a left fastener connecting the ith left rail element and a sleeper (Figure 2(a) and (b)), the upper end point has a dependent DOF depending on the vertical displacement, z_{Lr}, and rotation, ϑ_{xLr}, about the x-axis of the ith left rail element, while the lower end point also has a dependent DOF depending on the vertical displacement, z_s, and rotation, ϑ_{xs}, about the x-axis of the corresponding sleeper. The elastic strain energy of the vertical spring, $\Pi_{fas}^{\mathbf{LZ},e}$, can then be expressed as

$$
\begin{aligned}
\Pi_{fas}^{\mathbf{LZ},e} &= \frac{1}{2}\frac{k_{rsz}}{2}(z_{Lr}+b_{rt}\theta_{xLr}-z_s-(D_{rr}+b_{rt})\theta_{xs})^2+\frac{1}{2}\frac{k_{rsz}}{2}(z_{Lr}-b_{rt}\theta_{xLr}-z_s-(D_{rr}-b_{rt})\theta_{xs})^2 \\
&= \frac{1}{2}\frac{k_{rsz}}{2}(N_{rz,1}z_{Lr,i}+N_{rz,2}\theta_{yLr,i}+N_{rz,3}z_{Lr,i+1}+N_{rz,4}\theta_{yLr,i+1}+b_{rt}(N_{r\theta x,1}\theta_{xLr,i}+N_{r\theta x,2}\theta_{xLr,i+1})-z_s-(D_{rr}+b_{rt})\theta_{xs})^2 \\
&+ \frac{1}{2}\frac{k_{rsz}}{2}(N_{rz,1}z_{Lr,i}+N_{rz,2}\theta_{yLr,i}+N_{rz,3}z_{Lr,i+1}+N_{rz,4}\theta_{yLr,i+1}-b_{rt}(N_{r\theta x,1}\theta_{xLr,i}+N_{r\theta x,2}\theta_{xLr,i+1})-z_s-(D_{rr}-b_{rt})\theta_{xs})^2 \\
&= \frac{1}{2}\frac{k_{rsz}}{2}\begin{bmatrix} z_{Lr,i}\\ \theta_{yLr,i}\\ z_{Lr,i+1}\\ \theta_{yLr,i+1}\\ \theta_{xLr,i}\\ \theta_{xLr,i+1}\\ z_s\\ \theta_{xs}\end{bmatrix}^{\mathbf{T}}\times\left\{\begin{bmatrix} N_{rz,1}\\ N_{rz,2}\\ N_{rz,3}\\ N_{rz,4}\\ b_{rt}N_{r\theta x,1}\\ b_{rt}N_{r\theta x,2}\\ -1\\ -(D_{rr}+b_{rt})\end{bmatrix}\times\begin{bmatrix} N_{rz,1}\\ N_{rz,2}\\ N_{rz,3}\\ N_{rz,4}\\ b_{rt}N_{r\theta x,1}\\ b_{rt}N_{r\theta x,2}\\ -1\\ -(D_{rr}+b_{rt})\end{bmatrix}^{\mathbf{T}}+\begin{bmatrix} N_{rz,1}\\ N_{rz,2}\\ N_{rz,3}\\ N_{rz,4}\\ -b_{rt}N_{r\theta x,1}\\ -b_{rt}N_{r\theta x,2}\\ -1\\ -(D_{rr}-b_{rt})\end{bmatrix}\times\begin{bmatrix} N_{rz,1}\\ N_{rz,2}\\ N_{rz,3}\\ N_{rz,4}\\ -b_{rt}N_{r\theta x,1}\\ -b_{rt}N_{r\theta x,2}\\ -1\\ -(D_{rr}-b_{rt})\end{bmatrix}^{\mathbf{T}}\right\}\times\begin{bmatrix} z_{Lr,i}\\ \theta_{yLr,i}\\ z_{Lr,i+1}\\ \theta_{yLr,i+1}\\ \theta_{xLr,i}\\ \theta_{xLr,i+1}\\ z_s\\ \theta_{xs}\end{bmatrix} \\
&= \frac{1}{2}[z_{Lr,i}\ \ \theta_{yLr,i}\ \ z_{Lr,i+1}\ \ \theta_{yLr,i+1}\ \ \theta_{xLr,i}\ \ \theta_{xLr,i+1}\ \ z_s\ \ \theta_{xs}]\times\mathbf{k}_{fas}^{\mathbf{LZ},e}\times[z_{Lr,i}\ \ \theta_{yLr,i}\ \ z_{Lr,i+1}\ \ \theta_{yLr,i+1}\ \ \theta_{xLr,i}\ \ \theta_{xLr,i+1}\ \ z_s\ \ \theta_{xs}]^{\mathbf{T}}
\end{aligned}
\tag{1}
$$

with

$$\mathbf{k}_{fas}^{\mathbf{LZ},e} = k_{rsz}\begin{bmatrix} N_{rz,1}N_{rz,1} & N_{rz,1}N_{rz,2} & N_{rz,1}N_{rz,3} & N_{rz,1}N_{rz,4} & 0 & 0 & -N_{rz,1} & -D_{rr}N_{rz,1} \\ & N_{rz,2}N_{rz,2} & N_{rz,2}N_{rz,3} & N_{rz,2}N_{rz,4} & 0 & 0 & -N_{rz,2} & -D_{rr}N_{rz,2} \\ & & N_{rz,3}N_{rz,3} & N_{rz,3}N_{rz,4} & 0 & 0 & -N_{rz,3} & -D_{rr}N_{rz,3} \\ & & & N_{rz,4}N_{rz,4} & 0 & 0 & -N_{rz,4} & -D_{rr}N_{rz,4} \\ & & & & b_{rt}^2N_{r\theta x,1}N_{r\theta x,1} & b_{rt}^2N_{r\theta x,1}N_{r\theta x,2} & 0 & -b_{rt}^2N_{r\theta x,1} \\ & & \textit{symm.} & & & b_{rt}^2N_{r\theta x,2}N_{r\theta x,2} & 0 & -b_{rt}^2N_{r\theta x,2} \\ & & & & & & 1 & D_{rr} \\ & & & & & & & D_{rr}^2+b_{rt}^2 \end{bmatrix} \tag{2}$$

$$N_{rz,1} = 1-3(\xi_{rs}/l_{re})^2+2(\xi_{rs}/l_{re})^3 \qquad N_{rz,2} = \xi_{rs}[-1+2(\xi_{rs}/l_{re})-(\xi_{rs}/l_{re})^2]$$

$$N_{rz,3} = 3(\xi_{rs}/l_{re})^2-2(\xi_{rs}/l_{re})^3 \qquad N_{rz,4} = \xi_{rs}[-(\xi_{rs}/l_{re})^2+(\xi_{rs}/l_{re})]$$

$$N_{r\theta x,1} = 1-\xi_{rs}/l_{re} \qquad N_{r\theta x,2} = \xi_{rs}/l_{re}$$

where ξ_{rs} denotes the longitudinal distance between the left node of the ith left rail element and the discrete spring, and $\mathbf{k}_{fas}^{\mathbf{LZ},e}$ denotes the stiffness matrix of the vertical discrete spring for a left fastener.

Similarly, one end point of the lateral spring for a left fastener connecting the ith left rail element and a sleeper has a dependent DOF depending on the lateral displacement, y_{Lr}, and rotation, ϑ_{xLr}, about the x-axis of the ith left rail element, while the other end point has an independent DOF, i.e., the lateral displacement, y_s, of the corresponding sleeper (Figure 2(b) and (c)). The stiffness matrix of the lateral discrete spring for a left fastener, $\mathbf{k}_{fas}^{\mathbf{LY},e}$, can then be expressed as

$$\mathbf{k}_{fas}^{\mathbf{LY},e} = k_{rsy}\begin{bmatrix} N_{ry,1}N_{ry,1} & N_{ry,1}N_{ry,2} & N_{ry,1}N_{ry,3} & N_{ry,1}N_{ry,4} & h_{rt2}N_{ry,1}N_{r\theta x,1} & h_{rt2}N_{ry,1}N_{r\theta x,2} & -N_{ry,1} \\ & N_{ry,2}N_{ry,2} & N_{ry,2}N_{ry,3} & N_{ry,2}N_{ry,4} & h_{rt2}N_{ry,2}N_{r\theta x,1} & h_{rt2}N_{ry,2}N_{r\theta x,2} & -N_{ry,2} \\ & & N_{ry,3}N_{ry,3} & N_{ry,3}N_{ry,4} & h_{rt2}N_{ry,3}N_{r\theta x,1} & h_{rt2}N_{ry,3}N_{r\theta x,2} & -N_{ry,3} \\ & & & N_{ry,4}N_{ry,4} & h_{rt2}N_{ry,4}N_{r\theta x,1} & h_{rt2}N_{ry,4}N_{r\theta x,2} & -N_{ry,4} \\ & & & & h_{rt2}^2N_{r\theta x,1}N_{r\theta x,1} & h_{rt2}^2N_{r\theta x,1}N_{r\theta x,2} & -h_{rt2}N_{r\theta x,1} \\ & & \textit{symm.} & & & h_{rt2}^2N_{r\theta x,2}N_{r\theta x,2} & -h_{rt2}N_{r\theta x,2} \\ & & & & & & 1 \end{bmatrix} \tag{3}$$

with

$$N_{ry,1} = 1-3(\xi_{rs}/l_{re})^2+2(\xi_{rs}/l_{re})^3 \qquad N_{ry,2} = \xi_{rs}[1-2(\xi_{rs}/l_{re})+(\xi_{rs}/l_{re})^2]$$

$$N_{ry,3} = 3(\xi_{rs}/l_{re})^2-2(\xi_{rs}/l_{re})^3 \qquad N_{ry,4} = \xi_{rs}[(\xi_{rs}/l_{re})^2-(\xi_{rs}/l_{re})].$$

The vertical and lateral damping matrices, $\mathbf{c}_{fas}^{\mathbf{LZ},e}$ and $\mathbf{c}_{fas}^{\mathbf{LY},e}$, of the discrete damper for a left fastener can be obtained simply by replacing "k_{rsz}" and "k_{rsy}" in the corresponding stiffness matrices, $\mathbf{k}_{fas}^{\mathbf{LZ},e}$ and $\mathbf{k}_{fas}^{\mathbf{LY},e}$, using "$c_{rsz}$" and "$c_{rsy}$", respectively.

The vertical stiffness and damping matrices for a right fastener, $\mathbf{k}_{fas}^{\mathbf{RZ},e}$ and $\mathbf{c}_{fas}^{\mathbf{RZ},e}$, as well as the lateral stiffness and damping matrices, $\mathbf{k}_{fas}^{\mathbf{RY},e}$ and $\mathbf{c}_{fas}^{\mathbf{RY},e}$, can be obtained by following a procedure similar to that given above.

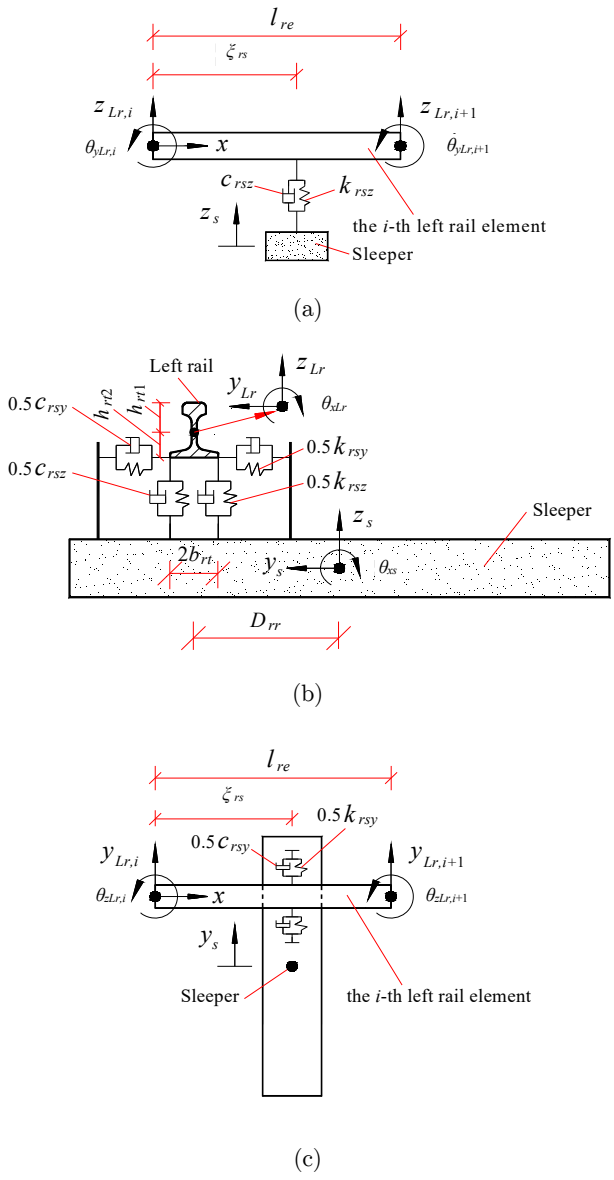

Figure 2: Sleeper attached to the ith left rail element by fastener: frontal view, (b) left side view, (c) top view.

2.3 Formulation of Stiffness and Damping Matrices of Ballast

For both the vertical and lateral discrete spring and damper representing a ballast, one end point connects to a sleeper, while the other end point connects to a bridge element, as shown in Figures 1 and 3. If we use as an example the vertical discrete spring in modeling a ballast connecting a sleeper, and the ith bridge element (Figure 3(a) and (b)), the upper end point has a dependent DOF that depends on the vertical displacement, z_s, and the rotation, ϑ_{xs}, about the x-axis of the sleeper, while the lower end point also has a dependent DOF depending on the vertical displacement, z_b, and the

rotation, ϑ_{xb}, about the x-axis of the ith bridge element. The stiffness matrix of the vertical discrete spring for a ballast, $\mathbf{k}_{bal}^{\mathbf{Z},e}$, can then be expressed as follows,

$$\mathbf{k}_{bal}^{\mathbf{Z},e} = 2k_{sbz}\begin{bmatrix} 1 & 0 & -N_{bz,1}^{s} & -N_{bz,2}^{s} & -N_{bz,3}^{s} & -N_{bz,4}^{s} & -D_{ctb}N_{b\theta x,1}^{s} & -D_{ctb}N_{b\theta x,2}^{s} \\ & D_{bal}^{2} & 0 & 0 & 0 & 0 & -D_{bal}^{2}N_{b\theta x,1}^{s} & -D_{bal}^{2}N_{b\theta x,2}^{s} \\ & & N_{bz,1}^{s}N_{bz,1}^{s} & N_{bz,1}^{s}N_{bz,2}^{s} & N_{bz,1}^{s}N_{bz,3}^{s} & N_{bz,1}^{s}N_{bz,4}^{s} & D_{ctb}N_{bz,1}^{s}N_{b\theta x,1}^{s} & D_{ctb}N_{bz,1}^{s}N_{b\theta x,2}^{s} \\ & & & N_{bz,2}^{s}N_{bz,2}^{s} & N_{bz,2}^{s}N_{bz,3}^{s} & N_{bz,2}^{s}N_{bz,4}^{s} & D_{ctb}N_{bz,2}^{s}N_{b\theta x,1}^{s} & D_{ctb}N_{bz,2}^{s}N_{b\theta x,2}^{s} \\ & & & & N_{bz,3}^{s}N_{bz,3}^{s} & N_{bz,3}^{s}N_{bz,4}^{s} & D_{ctb}N_{bz,3}^{s}N_{b\theta x,1}^{s} & D_{ctb}N_{bz,3}^{s}N_{b\theta x,2}^{s} \\ & & symm. & & & N_{bz,4}^{s}N_{bz,4}^{s} & D_{ctb}N_{bz,4}^{s}N_{b\theta x,1}^{s} & D_{ctb}N_{bz,4}^{s}N_{b\theta x,2}^{s} \\ & & & & & & (D_{ctb}^{2}+D_{bal}^{2})N_{b\theta x,1}^{s}N_{b\theta x,1}^{s} & (D_{ctb}^{2}+D_{bal}^{2})N_{b\theta x,1}^{s}N_{b\theta x,2}^{s} \\ & & & & & & & (D_{ctb}^{2}+D_{bal}^{2})N_{b\theta x,2}^{s}N_{b\theta x,2}^{s} \end{bmatrix} \tag{4}$$

with

$$N_{bz,1}^{s} = 1-3(\xi_{sb}/l_{be})^{2}+2(\xi_{sb}/l_{be})^{3} \qquad N_{bz,2}^{s} = \xi_{sb}[-1+2(\xi_{sb}/l_{be})-(\xi_{sb}/l_{be})^{2}]$$
$$N_{bz,3}^{s} = 3(\xi_{sb}/l_{be})^{2}-2(\xi_{sb}/l_{be})^{3} \qquad N_{bz,4}^{s} = \xi_{sb}[-(\xi_{sb}/l_{be})^{2}+(\xi_{sb}/l_{be})]$$
$$N_{b\theta x,1}^{s} = 1-\xi_{sb}/l_{be} \qquad N_{b\theta x,2}^{s} = \xi_{sb}/l_{be},$$

where ξ_{sb} denotes the longitudinal distance between the left node of the ith bridge element and the discrete spring.

Similarly, one end point of the lateral spring for a ballast connecting a sleeper and the ith bridge element has an independent DOF, i.e., the lateral displacement, y_s, of the sleeper, while the other end point has a dependent DOF depending on the lateral displacement, y_b, and the rotation, ϑ_{xb}, about the x-axis of the ith bridge element (Figure 3(b) and (c)). The stiffness matrix of the lateral discrete spring for a ballast, $\mathbf{k}_{bal}^{\mathbf{Y},e}$, can then be derived as follows,

$$\mathbf{k}_{bal}^{\mathbf{Y},e} = 2k_{sby}\begin{bmatrix} 1 & -N_{by,1}^{s} & -N_{by,2}^{s} & -N_{by,3}^{s} & -N_{by,4}^{s} & h_{bt1}N_{b\theta x,1}^{s} & h_{bt1}N_{b\theta x,2}^{s} \\ & N_{by,1}^{s}N_{by,1}^{s} & N_{by,1}^{s}N_{by,2}^{s} & N_{by,1}^{s}N_{by,3}^{s} & N_{by,1}^{s}N_{by,4}^{s} & -h_{bt1}N_{by,1}^{s}N_{b\theta x,1}^{s} & -h_{bt1}N_{by,1}^{s}N_{b\theta x,2}^{s} \\ & & N_{by,2}^{s}N_{by,2}^{s} & N_{by,2}^{s}N_{by,3}^{s} & N_{by,2}^{s}N_{by,4}^{s} & -h_{bt1}N_{by,2}^{s}N_{b\theta x,1}^{s} & -h_{bt1}N_{by,2}^{s}N_{b\theta x,2}^{s} \\ & & & N_{by,3}^{s}N_{by,3}^{s} & N_{by,3}^{s}N_{by,4}^{s} & -h_{bt1}N_{by,3}^{s}N_{b\theta x,1}^{s} & -h_{bt1}N_{by,3}^{s}N_{b\theta x,2}^{s} \\ & & & & N_{by,4}^{s}N_{by,4}^{s} & -h_{bt1}N_{by,4}^{s}N_{b\theta x,1}^{s} & -h_{bt1}N_{by,4}^{s}N_{b\theta x,2}^{s} \\ & symm. & & & & h_{bt1}^{2}N_{b\theta x,1}^{s}N_{b\theta x,1}^{s} & h_{bt1}^{2}N_{b\theta x,1}^{s}N_{b\theta x,2}^{s} \\ & & & & & & h_{bt1}^{2}N_{b\theta x,2}^{s}N_{b\theta x,2}^{s} \end{bmatrix} \tag{5}$$

with

$$N_{by,1}^{s} = 1-3(\xi_{sb}/l_{be})^{2}+2(\xi_{sb}/l_{be})^{3} \qquad N_{by,2}^{s} = \xi_{sb}[1-2(\xi_{sb}/l_{be})+(\xi_{sb}/l_{be})^{2}]$$
$$N_{by,3}^{s} = 3(\xi_{sb}/l_{be})^{2}-2(\xi_{sb}/l_{be})^{3} \qquad N_{by,4}^{s} = \xi_{sb}[(\xi_{sb}/l_{be})^{2}-(\xi_{sb}/l_{be})].$$

The vertical and lateral damping matrices, $\mathbf{c}_{bal}^{\mathbf{Z},e}$ and $\mathbf{c}_{bas}^{\mathbf{Y},e}$, of the discrete damper for a ballast can be obtained simply by replacing "k_{sbz}" and "k_{sby}" in the corresponding stiffness matrices, $\mathbf{k}_{bal}^{\mathbf{Z},e}$ and $\mathbf{k}_{bal}^{\mathbf{Y},e}$, using "$c_{sbz}$" and "$c_{sby}$", respectively.

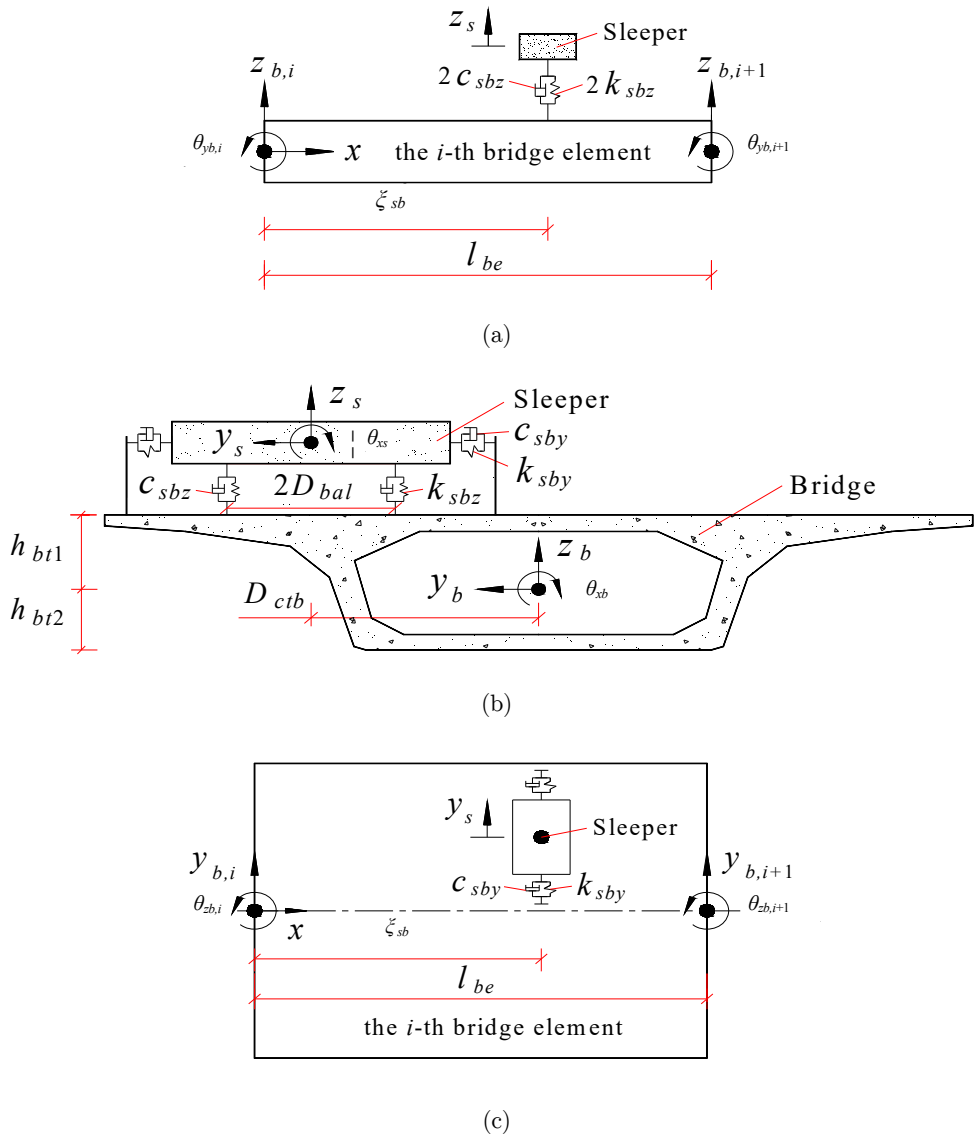

Figure 3: Sleeper attached to ith bridge element of by ballast: (a) frontal view, (b) left side view, (c) top view.

2.4 Formulation of Stiffness and Damping Matrices of Bearing

For both the vertical and lateral discrete springs and damper that represent a bearing, one end point connects a bridge element, while the other end point connects a node of the pier element, as shown in Figures 1 and 4. If we take the model of a vertical discrete spring and bearing connecting the ith bridge element and the ith node of pier element as an example (Figure 4(a) and (b)), the upper end point has a dependent DOF depending on the vertical displacement, z_b, and rotation, ϑ_{xb}, about the x-axis of the ith bridge element. In addition, the lower end point also has a dependent DOF relating to the vertical displacement, $z_{p,i}$, and rotation, $\vartheta_{xp,i}$, about the x-axis of the ith node of

the pier element. In this case, the stiffness matrix of the vertical discrete spring for a bearing, $\mathbf{k}_{bea}^{\mathbf{Z},e}$, can be expressed as

$$\mathbf{k}_{bea}^{\mathbf{Z},e} = 2k_{bbz}\begin{bmatrix} N_{bz,1}^b N_{bz,1}^b & N_{bz,1}^b N_{bz,2}^b & N_{bz,1}^b N_{bz,3}^b & N_{bz,1}^b N_{bz,4}^b & 0 & 0 & -N_{bz,1}^b & 0 \\ & N_{bz,2}^b N_{bz,2}^b & N_{bz,2}^b N_{bz,3}^b & N_{bz,2}^b N_{bz,4}^b & 0 & 0 & -N_{bz,2}^b & 0 \\ & & N_{bz,3}^b N_{bz,3}^b & N_{bz,3}^b N_{bz,4}^b & 0 & 0 & -N_{bz,3}^b & 0 \\ & & & N_{bz,4}^b N_{bz,4}^b & 0 & 0 & -N_{bz,4}^b & 0 \\ & & & & D_{cbb}^2 N_{b\theta x,1}^b N_{b\theta x,1}^b & D_{cbb}^2 N_{b\theta x,1}^b N_{b\theta x,2}^b & 0 & -D_{cbb}^2 N_{b\theta x,1}^b \\ & & \textit{symm.} & & & D_{cbb}^2 N_{b\theta x,2}^b N_{b\theta x,2}^b & 0 & -D_{cbb}^2 N_{b\theta x,2}^b \\ & & & & & & 1 & 0 \\ & & & & & & & D_{cbb}^2 \end{bmatrix} \tag{6}$$

with

$$N_{bz,1}^b = 1 - 3(\xi_{bb}/l_{be})^2 + 2(\xi_{bb}/l_{be})^3 \qquad N_{bz,2}^b = \xi_{bb}[-1 + 2(\xi_{bb}/l_{be}) - (\xi_{bb}/l_{be})^2]$$
$$N_{bz,3}^b = 3(\xi_{bb}/l_{be})^2 - 2(\xi_{bb}/l_{be})^3 \qquad N_{bz,4}^b = \xi_{bb}[-(\xi_{bb}/l_{be})^2 + (\xi_{bb}/l_{be})]$$
$$N_{b\theta x,1}^b = 1 - \xi_{bb}/l_{be} \qquad N_{b\theta x,2}^b = \xi_{bb}/l_{be},$$

where ξ_{bb} denotes the longitudinal distance between the left node of the ith bridge element and the discrete spring.

Similarly, one end point of the lateral spring for a bearing connecting the ith bridge element and the ith node of pier element has a dependent DOF in relation to the lateral displacement, y_b, and rotation, ϑ_{xb}, about the x-axis of the ith bridge element. In addition, the other end point has an independent DOF, i.e., the lateral displacement, $y_{p,i}$, of the corresponding node of the pier element (Figure 4(b)). The stiffness matrix of the lateral discrete spring for a bearing, $\mathbf{k}_{bea}^{\mathbf{Y},e}$, can then be expressed as

$$\mathbf{k}_{bea}^{\mathbf{Y},e} = 2k_{bby}\begin{bmatrix} N_{by,1}^b N_{by,1}^b & N_{by,1}^b N_{by,2}^b & N_{by,1}^b N_{by,3}^b & N_{by,1}^b N_{by,4}^b & h_{bt2} N_{by,1}^b N_{b\theta x,1}^b & h_{bt2} N_{by,1}^b N_{b\theta x,2}^b & -N_{by,1}^b \\ & N_{by,2}^b N_{by,2}^b & N_{by,2}^b N_{by,3}^b & N_{by,2}^b N_{by,4}^b & h_{bt2} N_{by,2}^b N_{b\theta x,1}^b & h_{bt2} N_{by,2}^b N_{b\theta x,2}^b & -N_{by,2}^b \\ & & N_{by,3}^b N_{by,3}^b & N_{by,3}^b N_{by,4}^b & h_{bt2} N_{by,3}^b N_{b\theta x,1}^b & h_{bt2} N_{by,3}^b N_{b\theta x,2}^b & -N_{by,3}^b \\ & & & N_{by,4}^b N_{by,4}^b & h_{bt2} N_{by,4}^b N_{b\theta x,1}^b & h_{bt2} N_{by,4}^b N_{b\theta x,2}^b & -N_{by,4}^b \\ & & & & h_{bt2}^2 N_{b\theta x,1}^b N_{b\theta x,1}^b & h_{bt2}^2 N_{b\theta x,1}^b N_{b\theta x,2}^b & -h_{bt2} N_{b\theta x,1}^b \\ & & \textit{symm.} & & & h_{bt2}^2 N_{b\theta x,2}^b N_{b\theta x,2}^b & -h_{bt2} N_{b\theta x,2}^b \\ & & & & & & 1 \end{bmatrix} \tag{7}$$

with

$$N_{by,1}^b = 1 - 3(\xi_{bb}/l_{be})^2 + 2(\xi_{bb}/l_{be})^3 \qquad N_{by,2}^b = \xi_{bb}[1 - 2(\xi_{bb}/l_{be}) + (\xi_{bb}/l_{be})^2]$$
$$N_{by,3}^b = 3(\xi_{bb}/l_{be})^2 - 2(\xi_{bb}/l_{be})^3 \qquad N_{by,4}^b = \xi_{bb}[(\xi_{bb}/l_{be})^2 - (\xi_{bb}/l_{be})].$$

The vertical and lateral damping matrices, $\mathbf{c}_{bea}^{\mathbf{Z},e}$ and $\mathbf{c}_{bea}^{\mathbf{Y},e}$, respectively, of the discrete damper for a bearing can then be obtained simply by replacing "k_{bbz}" and "k_{bby}" in the corresponding stiffness matrices, $\mathbf{k}_{bea}^{\mathbf{Z},e}$ and $\mathbf{k}_{bea}^{\mathbf{Y},e}$, with "$c_{bbz}$" and "$c_{bby}$", respectively.

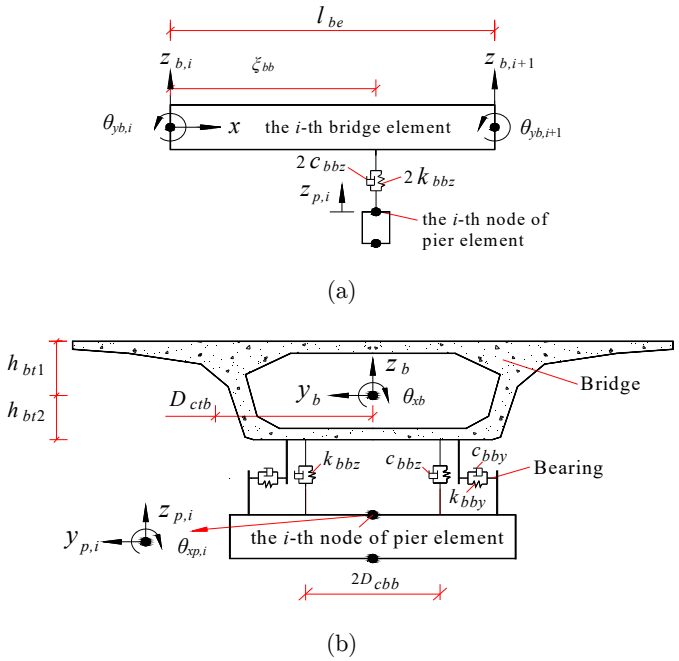

Figure 4: Bridge element attached to the *i*th node of pier element by bearing: (a) frontal view, (b) left side view.

3 3D EQUATIONS OF MOTION FOR A TTBI SYSTEM WITH PROPOSED ELEMENT

Figure 5 shows a train consisting of a series of four-wheelset vehicles moving with a constant speed, v_t, on a ballasted track structure that rests on a multi-span continuous beam bridge.

The train consists of N_v identical vehicles numbered 1, 2, ...N_v, from right to left. Each vehicle in the train is modeled as a mass-spring-damper system consisting of one carbody, two bogies, four wheelsets, and two-stage suspensions. The carbody is modeled as a rigid body with mass, m_c, and three moments of inertia, I_{cx}, I_{cy}, and I_{cz}. Similarly, each bogie is considered as a rigid body with mass, m_t, and three moments of inertia, I_{tx}, I_{ty}, and I_{tz}, and each wheelset is considered as a rigid body with mass, m_w, and two moments of inertia, I_{wx} and I_{wz}. The secondary suspension between the carbody and each bogie is characterized by a three-dimensional system of springs with stiffnesses k_{sx}, k_{sy}, and k_{sz} and dampers with damping coefficients c_{sx}, c_{sy}, and c_{sz}. Likewise, the springs and shock absorbers in the primary suspension for each wheelset are characterized by k_{px}, k_{py}, and k_{pz} and c_{px}, c_{py}, and c_{pz}, respectively. By neglecting longitudinal displacements, the motions of the carbody of the jth vehicle with respect to its center of gravity may be described by y_{cj}, z_{cj}, ϑ_{cj}, φ_{cj}, and ψ_{cj}. Similarly, the motions of both the front and rear bogies of the jth vehicle may be described by y_{t1j}, z_{t1j}, ϑ_{t1j}, φ_{t1j}, and ψ_{t1j} and y_{t2j}, z_{t2j}, ϑ_{t2j}, φ_{t2j}, and ψ_{t2j}, respectively. In addition, the motion from right to left of the hth (h = 1–4) wheelset of the jth vehicle may be described by y_{whj}, z_{whj}, ϑ_{whj}, and ψ_{whj}, respectively. In this paper however, it is assumed that no jumps occur between the vehicle's wheels and the rails; that is, the vertical and rolling displacements of each wheelset are constrained by the corresponding displacements of the rails. Consequently, each vehicle has 23 independent DOFs.

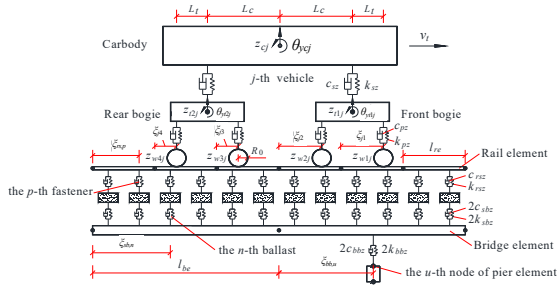

(a)

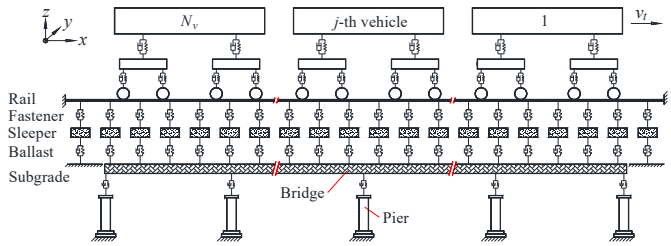

(b)

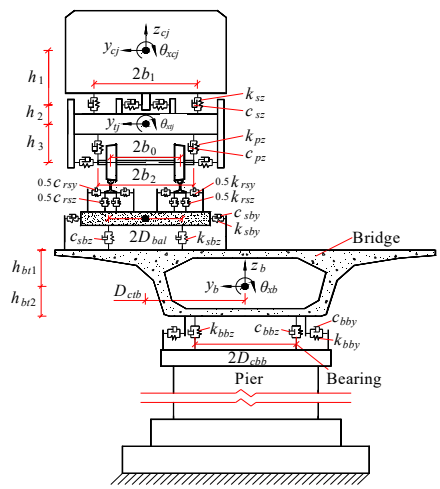

(c)

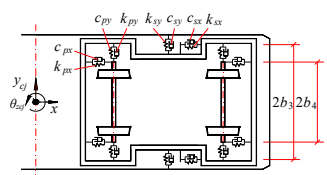

(d)

Figure 5: 3D model for TTBI system: (a) frontal view, (b) jth vehicle moving on rail–bridge coupling elements of unequal lengths, (c) left side view, (d) top view (without bridge).

By using the energy principle, such as the principle of the stationary value of total potential energy of a dynamic system (Zeng, 2000; Lou and Zeng, 2005), it is possible to derive the 3D equations of motion written in a sub-matrix for a TTBI system that is shown in Figure 5, as

$$\begin{bmatrix} \mathbf{M}_{tt} & 0 & 0 & 0 & 0 \\ 0 & \mathbf{M}_{rr} & 0 & 0 & 0 \\ 0 & 0 & \mathbf{M}_{ss} & 0 & 0 \\ 0 & 0 & 0 & \mathbf{M}_{bb} & 0 \\ 0 & 0 & 0 & 0 & \mathbf{M}_{pp} \end{bmatrix} \begin{bmatrix} \ddot{\mathbf{X}}_t \\ \ddot{\mathbf{X}}_r \\ \ddot{\mathbf{X}}_s \\ \ddot{\mathbf{X}}_b \\ \ddot{\mathbf{X}}_p \end{bmatrix} + \begin{bmatrix} \mathbf{C}_{tt} & \mathbf{C}_{tr} & 0 & 0 & 0 \\ \mathbf{C}_{rt} & \mathbf{C}_{rr} & \mathbf{C}_{rs} & 0 & 0 \\ 0 & \mathbf{C}_{sr} & \mathbf{C}_{ss} & \mathbf{C}_{sb} & 0 \\ 0 & 0 & \mathbf{C}_{bs} & \mathbf{C}_{bb} & \mathbf{C}_{bp} \\ 0 & 0 & 0 & \mathbf{C}_{pb} & \mathbf{C}_{pp} \end{bmatrix} \begin{bmatrix} \dot{\mathbf{X}}_t \\ \dot{\mathbf{X}}_r \\ \dot{\mathbf{X}}_s \\ \dot{\mathbf{X}}_b \\ \dot{\mathbf{X}}_p \end{bmatrix} + \begin{bmatrix} \mathbf{K}_{tt} & \mathbf{K}_{tr} & 0 & 0 & 0 \\ \mathbf{K}_{rt} & \mathbf{K}_{rr} & \mathbf{K}_{rs} & 0 & 0 \\ 0 & \mathbf{K}_{sr} & \mathbf{K}_{ss} & \mathbf{K}_{sb} & 0 \\ 0 & 0 & \mathbf{K}_{bs} & \mathbf{K}_{bb} & \mathbf{K}_{bp} \\ 0 & 0 & 0 & \mathbf{K}_{pb} & \mathbf{K}_{pp} \end{bmatrix} \begin{bmatrix} \mathbf{X}_t \\ \mathbf{X}_r \\ \mathbf{X}_s \\ \mathbf{X}_b \\ \mathbf{X}_p \end{bmatrix} = \begin{bmatrix} \mathbf{F}_t \\ \mathbf{F}_r \\ \mathbf{F}_s \\ \mathbf{F}_b \\ \mathbf{F}_p \end{bmatrix} \tag{8}$$

where the subscripts "*t*", "*r*", "*s*", "*b*", and "*p*" denote the train, rail, sleeper, bridge, and pier, respectively; $\mathbf{M}$, $\mathbf{C}$, and $\mathbf{K}$ denote the mass, damping, and stiffness sub-matrices, respectively; and $\mathbf{X}$ and $\mathbf{F}$ denote the displacement and force sub-vectors, respectively. The formation of equation (8) from terms in equations (2), (3), (4), (5), (6), and (7) is further explained below.

In order to build up equation (8), the stiffness matrices, $\mathbf{k}_{fas}^{\mathbf{LZ},e}$, in equation (2) and, $\mathbf{k}_{fas}^{\mathbf{LY},e}$, in equation (3) can be partitioned into four parts as follows,

$$\mathbf{k}_{fas}^{\mathbf{LZ},e} = \begin{bmatrix} \mathbf{k}_{fas}^{\mathbf{LZ},e1} & \mathbf{k}_{fas}^{\mathbf{LZ},e2} \\ \mathbf{k}_{fas}^{\mathbf{LZ},e3} & \mathbf{k}_{fas}^{\mathbf{LZ},e4} \end{bmatrix} \tag{9}$$

$$\mathbf{k}_{fas}^{\mathbf{LY},e} = \begin{bmatrix} \mathbf{k}_{fas}^{\mathbf{LY},e1} & \mathbf{k}_{fas}^{\mathbf{LY},e2} \\ \mathbf{k}_{fas}^{\mathbf{LY},e3} & \mathbf{k}_{fas}^{\mathbf{LY},e4} \end{bmatrix} \tag{10}$$

$$\mathbf{k}_{fas}^{\mathbf{LZ},e1} = k_{rsz} \begin{bmatrix} N_{rz,1}N_{rz,1} & N_{rz,1}N_{rz,2} & N_{rz,1}N_{rz,3} & N_{rz,1}N_{rz,4} & 0 & 0 \\ & N_{rz,2}N_{rz,2} & N_{rz,2}N_{rz,3} & N_{rz,2}N_{rz,4} & 0 & 0 \\ & & N_{rz,3}N_{rz,3} & N_{rz,3}N_{rz,4} & 0 & 0 \\ & & & N_{rz,4}N_{rz,4} & 0 & 0 \\ & \textit{symm.} & & & b_{rt}^2 N_{r\theta x,1}N_{r\theta x,1} & b_{rt}^2 N_{r\theta x,1}N_{r\theta x,2} \\ & & & & & b_{rt}^2 N_{r\theta x,2}N_{r\theta x,2} \end{bmatrix} \tag{11}$$

$$\mathbf{k}_{fas}^{\mathbf{LZ},e2} = k_{rsz} \begin{bmatrix} -N_{rz,1} & -N_{rz,2} & -N_{rz,3} & -N_{rz,4} & 0 & 0 \\ -D_{rr}N_{rz,1} & -D_{rr}N_{rz,2} & -D_{rr}N_{rz,3} & -D_{rr}N_{rz,4} & -b_{rt}^2 N_{r\theta x,1} & -b_{rt}^2 N_{r\theta x,2} \end{bmatrix}^{\mathbf{T}} \tag{12}$$

$$\mathbf{k}_{fas}^{\mathbf{LZ},e3} = k_{rsz} \begin{bmatrix} -N_{rz,1} & -N_{rz,2} & -N_{rz,3} & -N_{rz,4} & 0 & 0 \\ -D_{rr}N_{rz,1} & -D_{rr}N_{rz,2} & -D_{rr}N_{rz,3} & -D_{rr}N_{rz,4} & -b_{rt}^2 N_{r\theta x,1} & -b_{rt}^2 N_{r\theta x,2} \end{bmatrix} \tag{13}$$

$$\mathbf{k}_{fas}^{\mathbf{LZ},e4} = k_{rsz} \begin{bmatrix} 1 & D_{rr} \\ D_{rr} & D_{rr}^2 + b_{rt}^2 \end{bmatrix} \tag{14}$$

$$\mathbf{k}_{fas}^{\mathbf{LY},e1} = k_{rsy} \begin{bmatrix} N_{ry,1}N_{ry,1} & N_{ry,1}N_{ry,2} & N_{ry,1}N_{ry,3} & N_{ry,1}N_{ry,4} & h_{rt2}N_{ry,1}N_{r\theta x,1} & h_{rt2}N_{ry,1}N_{r\theta x,2} \\ & N_{ry,2}N_{ry,2} & N_{ry,2}N_{ry,3} & N_{ry,2}N_{ry,4} & h_{rt2}N_{ry,2}N_{r\theta x,1} & h_{rt2}N_{ry,2}N_{r\theta x,2} \\ & & N_{ry,3}N_{ry,3} & N_{ry,3}N_{ry,4} & h_{rt2}N_{ry,3}N_{r\theta x,1} & h_{rt2}N_{ry,3}N_{r\theta x,2} \\ & & & N_{ry,4}N_{ry,4} & h_{rt2}N_{ry,4}N_{r\theta x,1} & h_{rt2}N_{ry,4}N_{r\theta x,2} \\ & \textit{symm.} & & & h_{rt2}^2 N_{r\theta x,1}N_{r\theta x,1} & h_{rt2}^2 N_{r\theta x,1}N_{r\theta x,2} \\ & & & & & h_{rt2}^2 N_{r\theta x,2}N_{r\theta x,2} \end{bmatrix} \tag{15}$$

$$\mathbf{k}_{fas}^{\mathbf{LY},e2} = k_{rsy}[-N_{ry,1} \ -N_{ry,2} \ -N_{ry,3} \ -N_{ry,4} \ -h_{rt2}N_{r\theta x,1} \ -h_{rt2}N_{r\theta x,2}]^{\mathbf{T}} \tag{16}$$

$$\mathbf{k}_{fas}^{\mathbf{LY},e3} = k_{rsy}[-N_{ry,1} \ -N_{ry,2} \ -N_{ry,3} \ -N_{ry,4} \ -h_{rt2}N_{r\theta k,1} \ -h_{rt2}N_{r\theta k,2}] \tag{17}$$

and

$$\mathbf{k}_{fas}^{\mathbf{LY},e4} = k_{rsy} \tag{18}$$

Elements in matrices $\mathbf{k}_{fas}^{\mathbf{LZ},e1}$ and $\mathbf{k}_{fas}^{\mathbf{LY},e1}$ should be placed in the stiffness sub-matrix $\mathbf{K}_{Lrr}$ (see equation (27)); elements in matrices $\mathbf{k}_{fas}^{\mathbf{LZ},e2}$ and $\mathbf{k}_{fas}^{\mathbf{LY},e2}$ should be placed in the stiffness sub-matrix $\mathbf{K}_{Lrs}$; elements in matrices $\mathbf{k}_{fas}^{\mathbf{LZ},e3}$ and $\mathbf{k}_{fas}^{\mathbf{LY},e3}$ should be placed in the stiffness sub-matrix $\mathbf{K}_{sLr}$; and elements in matrices $\mathbf{k}_{fas}^{\mathbf{LZ},e4}$ and $\mathbf{k}_{fas}^{\mathbf{LY},e4}$ should be placed in the stiffness sub-matrix $\mathbf{K}_{ss}$. Furthermore, in a similar manner to $\mathbf{k}_{fas}^{\mathbf{LZ},e}$ and $\mathbf{k}_{fas}^{\mathbf{LY},e}$, the damping matrices, $\mathbf{c}_{fas}^{\mathbf{LZ},e}$ and $\mathbf{c}_{fas}^{\mathbf{LY},e}$, can be partitioned into four parts and placed in the damping sub-matrices, $\mathbf{C}_{Lrr}$, $\mathbf{C}_{Lrs}$, $\mathbf{C}_{sLr}$, and $\mathbf{C}_{ss}$, respectively.

The stiffness matrix, $\mathbf{k}_{fas}^{\mathbf{RZ},e}$, can be partitioned into four parts and used as follows in building equation (8). Elements in the first six rows and the first six columns should be placed in the stiffness sub-matrix $\mathbf{K}_{Rrr}$; elements in the first six rows and the last two columns should be placed in the stiffness sub-matrix $\mathbf{K}_{Rrs}$; elements in the first six columns and the last two rows should be placed in the stiffness sub-matrix $\mathbf{K}_{sRr}$; and the remaining elements should be placed in the stiffness sub-matrix $\mathbf{K}_{ss}$.

The stiffness matrix, $\mathbf{k}_{fas}^{\mathbf{RY},e}$, can be partitioned into four parts and used as follows in building up equation (8). Elements in the first six rows and the first six columns should be placed in the stiffness sub-matrix $\mathbf{K}_{Rrr}$; elements in the first six rows and the last column should be placed in the stiffness sub-matrix $\mathbf{K}_{Rrs}$; elements in the first six columns and the last row should be placed in the stiffness sub-matrix $\mathbf{K}_{sRr}$; and the remaining element should be placed in the stiffness sub-matrix $\mathbf{K}_{ss}$. In a similar manner as $\mathbf{k}_{fas}^{\mathbf{RZ},e}$ and $\mathbf{k}_{fas}^{\mathbf{RY},e}$, the damping matrices, $\mathbf{c}_{fas}^{\mathbf{RZ},e}$ and $\mathbf{c}_{fas}^{\mathbf{RY},e}$, can be partitioned into four parts and placed in the damping sub-matrices, $\mathbf{C}_{Rrr}$, $\mathbf{C}_{Rrs}$, $\mathbf{C}_{sRr}$, and $\mathbf{C}_{ss}$, respectively.

Furthermore, the stiffness matrix, $\mathbf{k}_{bal}^{\mathbf{Z},e}$, in equation (4) can be partitioned into four parts and used as follows in building up equation (8). Elements in the first two rows and the first two columns should be placed in the in the stiffness sub-matrix $\mathbf{K}_{ss}$; elements in the first two rows and the last six columns should be placed in the stiffness sub-matrix $\mathbf{K}_{sb}$; elements in the first two columns and the last six rows should be placed in the stiffness sub-matrix $\mathbf{K}_{bs}$; and the remaining elements should be placed in the stiffness sub-matrix $\mathbf{K}_{bb}$.

The stiffness matrix, $\mathbf{k}_{bal}^{\mathbf{Y},e}$, in equation (5) can be partitioned into four parts as follows and used as follows in building up equation (8). Elements in the first row and the first column should be placed in the in the stiffness sub-matrix $\mathbf{K}_{ss}$; elements in the first row and the last six columns should be placed in the stiffness sub-matrix $\mathbf{K}_{sb}$; elements in the first column and the last six rows should be placed in the stiffness sub-matrix $\mathbf{K}_{bs}$; and the remaining elements should be placed in the stiffness sub-matrix $\mathbf{K}_{bb}$. In a similar manner as $\mathbf{k}_{bal}^{\mathbf{Z},e}$ and $\mathbf{k}_{bal}^{\mathbf{Y},e}$, the damping matrices, $\mathbf{c}_{bal}^{\mathbf{Z},e}$ and $\mathbf{c}_{bal}^{\mathbf{Y},e}$, can be partitioned into four parts and placed in the damping sub-matrices, $\mathbf{C}_{ss}$, $\mathbf{C}_{sb}$, $\mathbf{C}_{bs}$, and $\mathbf{C}_{bb}$, respectively.

The stiffness matrix, $\mathbf{k}_{bea}^{\mathbf{Z},e}$, in equation (6) can be partitioned into four parts and used as follows in building up equation (8). Elements in the first six rows and the first six columns should be placed in the stiffness sub-matrix $\mathbf{K}_{bb}$; elements in the first six rows and the last two columns should be placed in the stiffness sub-matrix $\mathbf{K}_{bp}$; elements in the first six columns and the last two rows should be placed in the stiffness sub-matrix $\mathbf{K}_{pb}$; and the remaining elements should be placed in the stiffness sub-matrix $\mathbf{K}_{pp}$.

The stiffness matrix, $\mathbf{k}_{bea}^{\mathbf{Y},e}$, in equation (7) can be partitioned into four parts and used as follows in building up equation (8). Elements in the first six rows and the first six columns should be placed in the stiffness sub-matrix $\mathbf{K}_{bb}$; elements in the first six rows and the last column should be placed in the stiffness sub-matrix $\mathbf{K}_{bp}$; elements in the first six columns and the last row should be placed in the stiffness sub-matrix $\mathbf{K}_{pb}$; and the remaining elements should be placed in the stiffness sub-matrix $\mathbf{K}_{pp}$. In a similar manner as $\mathbf{k}_{bea}^{\mathbf{Z},e}$ and $\mathbf{k}_{bea}^{\mathbf{Y},e}$, the damping matrices, $\mathbf{c}_{bea}^{\mathbf{Z},e}$ and $\mathbf{c}_{bea}^{\mathbf{Y},e}$, can be partitioned into four parts and placed in the damping sub-matrices, $\mathbf{C}_{bb}$, $\mathbf{C}_{bp}$, $\mathbf{C}_{pb}$, and $\mathbf{C}_{pp}$, respectively.

The displacement sub-vectors, the mass, damping, and stiffness sub-matrices, as well as the force sub-vectors of the train, rail, sleeper, bridge, and pier are explained briefly in the following sections, and a detailed explanation is found in Lou (2005, 2007) and Lou and Zeng (2005).

3.1 Displacement Vectors

The displacement sub-vector of the total train, $\mathbf{X}_t$, of order $T_{dof} \times 1$ ($T_{dof} = 23 \times N_v$) can be written as

$$\mathbf{X}_t = [\mathbf{X}_{v1}\ \mathbf{X}_{v2}\ \cdots\ \mathbf{X}_{vN_v}]^{\mathbf{T}} \tag{19}$$

where the superscript "$\mathbf{T}$" denotes the transpose of the matrix, and $\mathbf{X}_{vj}$ (j = 1, 2, ..., N_v) are the displacement vectors of the jth vehicle, which can be expressed as

$$\mathbf{X}_{vj} = [y_{cj}\ z_{cj}\ \theta_{xcj}\ \theta_{ycj}\ \theta_{zcj}\ y_{t1j}\ z_{t1j}\ \theta_{xt1j}\ \theta_{yt1j}\ \theta_{zt1j}\ y_{t2j}\ z_{t2j}\ \theta_{xt2j}\ \theta_{yt2j}\ \theta_{zt2j}\ y_{w1j}\ \theta_{zw1j}\ y_{w2j}\ \theta_{zw2j}\ y_{w3j}\ \theta_{zw3j}\ y_{w4j}\ \theta_{zw4j}]\,.$$

The displacement sub-vector of the rail, $\mathbf{X}_r$, of order $2\overline{N}_r \times 1$, which is composed of the displacement vectors $\mathbf{X}_{Lr}$ of the left rail of order $1 \times \overline{N}_r$, and $\mathbf{X}_{Rr}$ of the right rail of order $1 \times \overline{N}_r$, can be written as

$$\begin{aligned} \mathbf{X}_r &= [\mathbf{X}_{Lr}\ \mathbf{X}_{Rr}]^{\mathbf{T}} \\ \mathbf{X}_{Lr} &= \mathbf{X}_{Rr} = [q_{r1}\ q_{r2}\ \cdots\ q_{r\overline{N}_r}] \end{aligned} \tag{20}$$

where $\overline{N}_r$ denotes the total number of DOFs of each rail.

The displacement sub-vector of the sleeper, $\mathbf{X}_s$, of order $\overline{N}_s \times 1$ can be written as

$$\mathbf{X}_s = [\mathbf{X}_{s1}\ \mathbf{X}_{s2}\ \cdots\ \mathbf{X}_{sN_s}]^{\mathbf{T}} \tag{21}$$

where $\mathbf{x}_{si}$ (i = 1, 2, ..., N_s) of order 3 denotes the displacement vector of the ith sleeper, N_s denotes the total number of sleepers, and $\overline{N}_s$ denotes the total number of DOFs of all sleepers with $\overline{N}_s = 3N_s$. The displacement vector, $\mathbf{x}_{si}$, can be expressed as

$$\mathbf{x}_{si} = [y_{si} \;\; z_{si} \;\; \theta_{xsi}] .$$

The displacement sub-vector, $\mathbf{x}_b$, of order $\overline{N}_b \times 1$ for multi-span continuous beams used to model the bridge can be written as

$$\mathbf{X}_b = [\mathbf{X}_{b1} \;\; \mathbf{X}_{b2} \;\; \cdots \;\; \mathbf{X}_{bN_b}]^{\mathbf{T}} \tag{22}$$

where $\mathbf{x}_{bi}$ (i = 1, 2, ..., N_b) denotes the displacement vector of the ith bridge, N_b denotes the total number of bridges, and $\overline{N}_b$ denotes the total number of DOFs of all bridges. The displacement vector, $\mathbf{x}_{bi}$, of order $1 \times \overline{n}_{bi}$, and the number of DOFs, $\overline{N}_b$, can be expressed as

$$\mathbf{X}_{bi} = [q_{b1} \;\; q_{b2} \;\; \cdots \;\; q_{b\overline{n}_{bi}}]$$

$$\overline{N}_b = \sum_{i=1}^{N_b} \overline{n}_{bi} ,$$

where $\overline{n}_{bi}$ denotes the total number of DOFs of the ith bridge.

The displacement sub-vector of the pier, $\mathbf{x}_p$, of order $\overline{N}_p \times 1$ can be written as

$$\mathbf{X}_p = [\mathbf{X}_{p1} \;\; \mathbf{X}_{p2} \;\; \cdots \;\; \mathbf{X}_{pN_p}]^{\mathbf{T}} \tag{23}$$

where $\mathbf{x}_{pi}$ (i = 1, 2, ..., N_p) denotes the displacement vector of the ith pier, N_p denotes the total number of piers, and $\overline{N}_p$ denotes the total number of DOFs of all piers. The displacement vector, $\mathbf{x}_{pi}$, of order $1 \times \overline{n}_{pi}$ and the number of DOFs, $\overline{N}_p$, can be expressed as

$$\mathbf{X}_{pi} = [q_{p1} \;\; q_{p2} \;\; \cdots \;\; q_{p\overline{n}_{pi}}] ,$$

$$\overline{N}_p = \sum_{i=1}^{N_p} \overline{n}_{pi}$$

where $\overline{n}_{pi}$ denotes the total number of DOFs of the ith pier.

3.2 Sub-Matrices of Train

The sub-matrices of the train are marked with the subscript "tt". The mass sub-matrix, $\mathbf{M}_{tt}$, of the train of order $(23 \times N_v) \times (23 \times N_v)$ can be written as

$$\mathbf{M}_{tt} = \text{diag}\,[\mathbf{M}_{v1} \;\; \mathbf{M}_{v2} \;\; \cdots \;\; \mathbf{M}_{vN_v}] \tag{24}$$

where $\mathbf{M}_{vj}$ (j = 1, 2, ..., N_v) of order 23×23 denotes the mass matrix of the jth vehicle, and can be expressed as

$$\mathbf{M}_{vj} = \text{diag}[m_c \;\; m_c \;\; I_{cx} \;\; I_{cy} \;\; I_{cz} \;\; m_t \;\; m_t \;\; I_{tx} \;\; I_{ty} \;\; I_{tz} \;\; m_t \;\; m_t \;\; I_{tx} \;\; I_{ty} \;\; I_{tz} \;\; m_w \;\; I_{wz} \;\; m_w \;\; I_{wz} \;\; m_w \;\; I_{wz} \;\; m_w \;\; I_{wz}] .$$

The stiffness sub-matrix, $\mathbf{K}_{tt}$, of the train of order $(23\times N_v)\times(23\times N_v)$ can be written as

$$\mathbf{K}_{tt}=\text{diag}\,[\mathbf{K}_{v1}\ \ \mathbf{K}_{v2}\ \ \cdots\ \ \mathbf{K}_{vN_v}] \tag{25}$$

where $\mathbf{K}_{vj}\,(j=1,\,2,\,...,\,N_v)$ of order 23×23 denotes the stiffness matrix of the jth vehicle, and can be expressed by the stiffness of the suspension systems of the jth vehicle.

The damping sub-matrix, $\mathbf{C}_{tt}$, of the train of order $(23\times N_v)\times(23\times N_v)$ can be obtained by simply replacing k in the corresponding stiffness sub-matrix, $\mathbf{K}_{tt}$, with c.

3.3 Sub-Matrices of Rail

The matrices of the rail are marked with the subscript "rr". The mass sub-matrix of the rail, $\mathbf{M}_{rr}$, of order $2\overline{N}_r\times2\overline{N}_r$, composed of the mass matrices of the left and right rails, $\mathbf{M}_{Lrr}$ and $\mathbf{M}_{Rrr}$, respectively, both of order $\overline{N}_r\times\overline{N}_r$, can be written as

$$\begin{aligned}\mathbf{M}_{rr}&=\text{diag}[\mathbf{M}_{Lrr}\ \ \mathbf{M}_{Rrr}]\\ \mathbf{M}_{Lrr}&=\mathbf{M}_{Rrr}=\mathbf{M}_{rr1}+\mathbf{M}_{rr2}+\mathbf{M}_{rr3}+\mathbf{M}_{rr4}\end{aligned} \tag{26}$$

with

$$\mathbf{M}_{rr1}=\sum_{g=1}^{n_r}\int_0^{l_{rg}}\overline{m}_r\mathbf{N}_{ry,eg}^{\mathrm{T}}\mathbf{N}_{ry,eg}\,d\xi$$

$$\mathbf{M}_{rr2}=\sum_{g=1}^{n_r}\int_0^{l_{rg}}\overline{m}_r\mathbf{N}_{rz,eg}^{\mathrm{T}}\mathbf{N}_{rz,eg}\,d\xi$$

$$\mathbf{M}_{rr3}=\sum_{g=1}^{n_r}\int_0^{l_{rg}}\frac{\overline{m}_rI_{rx}}{A_r}\mathbf{N}_{r\theta,eg}^{\mathrm{T}}\mathbf{N}_{r\theta,eg}\,d\xi$$

$$\mathbf{M}_{rr4}=\sum_{j=1}^{N_v}\sum_{h=1}^{4}\frac{m_w}{2}\mathbf{N}_{zjh}^{\mathrm{T}}\mathbf{N}_{zjh}$$

$$\mathbf{N}_{ry,eg}=[0\ \ 0\ \cdots\ N_{ry,1}\ \ 0\ \ 0\ \ 0\ \ N_{ry,2}\ \ N_{ry,3}\ \ 0\ \ 0\ \ 0\ \ N_{ry,4}\ \cdots\ \ 0\ \ 0]$$

$$\mathbf{N}_{rz,eg}=[0\ \ 0\ \cdots\ \ 0\ \ N_{rz,1}\ \ 0\ \ N_{rz,2}\ \ 0\ \ 0\ \ N_{rz,3}\ \ 0\ \ N_{rz,4}\ \ 0\ \cdots\ \ 0\ \ 0]$$

$$\mathbf{N}_{r\theta,eg}=[0\ \ 0\ \cdots\ \ 0\ \ 0\ \ N_{r\theta x,1}\ \ 0\ \ 0\ \ 0\ \ 0\ \ N_{r\theta x,2}\ \ 0\ \ 0\ \cdots\ \ 0\ \ 0]$$

$$\mathbf{N}_{zjh}=[0\ \ 0\ \cdots\ \ 0\ \ N_{rz,1}\ \ 0\ \ N_{rz,2}\ \ 0\ \ 0\ \ N_{rz,3}\ \ 0\ \ N_{rz,4}\ \ 0\ \cdots\ \ 0\ \ 0]_{\xi=\xi_{jh}},$$

where $\mathbf{M}_{rr1}$, $\mathbf{M}_{rr2}$, and $\mathbf{M}_{rr3}$ denote the overall mass matrices in the xy plane, in the xz plane, and rotation about the x-axis of the rail itself, respectively; $\mathbf{M}_{rr4}$ denotes the overall mass matrix induced by the wheel masses of all vehicles; $\overline{m}_r$ denotes the mass per unit length of the rail; A_r denotes the cross-sectional area of the rail; I_{rx} denotes the torsional moment of inertia of the rail about the x-axis; n_r denotes the total number of elements of each rail; ξ denotes the local coordinate measured from the left node of a rail element; $\mathbf{N}_{ry,eg}$, $\mathbf{N}_{rz,eg}$, and $\mathbf{N}_{r\theta,eg}$ of order $1\times\overline{N}_r$ are the shape function vectors in the xy plane, the xz plane, and in rotation about the x-axis for the gth rail element, respectively. In addition, each element in $\mathbf{N}_{ry,eg}$, $\mathbf{N}_{rz,eg}$, and $\mathbf{N}_{r\theta,eg}$ is zero except those corresponding to the DOFs, respectively, in the xy plane, the xz plane, and in rotation about the x-axis of the two nodes of the gth rail element; $\mathbf{N}_{zjh}$ of order $1\times\overline{N}_r$ denotes the time-dependent shape function vector in the xz plane for the rail element, which is evaluated at the position of the hth wheel-

set of the jth vehicle; ξ_{j1}, ξ_{j2}, ξ_{j3}, and ξ_{j4} denote, respectively, the distances between the 1st, 2nd, 3rd, and 4th wheelsets of the jth vehicle and the left node of the rail element on which the wheelsets are acting. Furthermore, each element in $\mathbf{N}_{zjh}$ is zero except for those corresponding to the four DOFs in the xz plane of the two nodes of the rail element on which the hth wheelset of the jth vehicle is acting.

The stiffness sub-matrix of the rail, $\mathbf{K}_{rr}$, of order $2\overline{N}_r \times 2\overline{N}_r$, which is composed of the stiffness matrices of the left and right rails, $\mathbf{K}_{Lrr}$ and $\mathbf{K}_{Rrr}$, of order $\overline{N}_r \times \overline{N}_r$, and the left rail–right rail interaction stiffness matrices, $\mathbf{K}_{LrRr}$ and $\mathbf{K}_{RrLr}$, of order $\overline{N}_r \times \overline{N}_r$, can be written as

$$\begin{gathered}\mathbf{K}_{rr}=\begin{bmatrix}\mathbf{K}_{Lrr} & \mathbf{K}_{LrRr}\\ \mathbf{K}_{RrLr} & \mathbf{K}_{Rrr}\end{bmatrix}\\ \mathbf{K}_{Lrr}=\mathbf{K}_{Rrr}=\mathbf{K}_{rr1}+\mathbf{K}_{rr2}+\mathbf{K}_{rr3}+\mathbf{K}_{rr4}+\mathbf{K}_{rr5}+\mathbf{K}_{rr6}+\mathbf{K}_{rr7}+\mathbf{K}_{rr8}\\ \mathbf{K}_{LrRr}=\mathbf{K}_{RrLr}^{\mathbf{T}}\end{gathered} \tag{27}$$

with

$$\mathbf{K}_{rr1}=\sum_{g=1}^{n_r}\int_0^{l_{rz}} E_r I_{rz}\mathbf{N}''^{\mathbf{T}}_{ry,eg}\mathbf{N}''_{ry,eg}\,d\xi$$

$$\mathbf{K}_{rr2}=\sum_{g=1}^{n_r}\int_0^{l_{rz}} E_r I_{ry}\mathbf{N}''^{\mathbf{T}}_{rz,eg}\mathbf{N}''_{rz,eg}\,d\xi$$

$$\mathbf{K}_{rr3}=\sum_{g=1}^{n_r}\int_0^{l_{rz}} G_r I_{rx}\mathbf{N}'^{\mathbf{T}}_{r\theta,eg}\mathbf{N}'_{r\theta,eg}\,d\xi$$

$$\mathbf{K}_{rr4}=\sum_{j=1}^{N_v}\sum_{h=1}^{4} k_{pz}\mathbf{N}^{\mathbf{T}}_{zjh}\mathbf{N}_{zjh}$$

$$\mathbf{K}_{rr5}=\sum_{j=1}^{N_v}\sum_{h=1}^{4}\frac{W_{axle}\lambda}{4b_0}(\mathbf{N}^{\mathbf{T}}_{yjh}\mathbf{N}_{yjh}+h_{rt1}^2\mathbf{N}^{\mathbf{T}}_{\theta jh}\mathbf{N}_{\theta jh})$$

$$\mathbf{K}_{rr6}=\sum_{p=1}^{n_f} k_{rsy}\mathbf{N}^{\mathbf{T}}_{ry,p}\mathbf{N}_{ry,p}$$

$$\mathbf{K}_{rr7}=\sum_{p=1}^{n_f} k_{rsz}\mathbf{N}^{\mathbf{T}}_{rz,p}\mathbf{N}_{rz,p}$$

$$\mathbf{K}_{rr8}=\sum_{p=1}^{n_f} b_{r1}k_{rsz}\mathbf{N}^{\mathbf{T}}_{r\theta,p}\mathbf{N}_{r\theta,p}$$

$$\mathbf{K}_{LrRr}=\sum_{j=1}^{N_v}\sum_{h=1}^{4}\frac{W_{axle}\lambda}{4b_0}(-\mathbf{N}^{\mathbf{T}}_{yjh}\mathbf{N}_{yjh}+h_{rt1}\mathbf{N}^{\mathbf{T}}_{yjh}\mathbf{N}_{\theta jh}+h_{rt1}\mathbf{N}^{\mathbf{T}}_{\theta jh}\mathbf{N}_{yjh}-h_{rt1}^2\mathbf{N}^{\mathbf{T}}_{\theta jh}\mathbf{N}_{\theta jh})$$

$$\mathbf{N}_{yjh}=[0\ 0\ \cdots\ N_{ry,1}\ 0\ 0\ 0\ N_{ry,2}\ N_{ry,3}\ 0\ 0\ 0\ N_{ry,4}\ \cdots\ 0\ 0]_{\xi=\xi_{jh}}$$

$$\mathbf{N}_{\theta jh}=[0\ 0\ \cdots\ 0\ 0\ N_{r\theta x,1}\ 0\ 0\ 0\ 0\ N_{r\theta x,2}\ 0\ 0\ \cdots\ 0\ 0]_{\xi=\xi_{jh}}$$

$$\mathbf{N}_{ry,p}=[0\ 0\ \cdots\ N_{ry,1}\ 0\ 0\ 0\ N_{ry,2}\ N_{ry,3}\ 0\ 0\ 0\ N_{ry,4}\ \cdots\ 0\ 0]_{\xi=\xi_{r,p}}$$

$$\mathbf{N}_{rz,p}=[0\ 0\ \cdots\ 0\ N_{rz,1}\ 0\ N_{rz,2}\ 0\ 0\ N_{rz,3}\ 0\ N_{rz,4}\ 0\ \cdots\ 0\ 0]_{\xi=\xi_{r,p}}$$

$$\mathbf{N}_{r\theta,p}=[0\ 0\ \cdots\ 0\ 0\ N_{r\theta x,1}\ 0\ 0\ 0\ 0\ N_{r\theta x,2}\ 0\ 0\ \cdots\ 0\ 0]_{\xi=\xi_{r,p}},$$

where $\mathbf{K}_{rr1}$, $\mathbf{K}_{rr2}$, and $\mathbf{K}_{rr3}$ denote the overall stiffness matrices in the xy plane, the xz plane, and in rotation about the x-axis of the rail itself, respectively; $\mathbf{K}_{rr4}$ denotes the overall stiffness matrix induced by the vertical displacement of all vehicles; $\mathbf{K}_{rr5}$ denotes the overall stiffness matrix in-

duced by the train's weight; $\mathbf{K}_{rr6}$, $\mathbf{K}_{rr7}$, and $\mathbf{K}_{rr8}$ denote, respectively, the lateral, vertical, and torsional stiffness matrices induced by the stiffness of all fasteners; $\mathbf{K}_{LrRr}$ denotes the left rail–right rail interaction stiffness matrix induced by the train's weight; E_r denotes Young's modulus of the rail; G_r denotes the shear modulus of the rail; I_{ry} and I_{rz} denote the flexural moments of inertia about the y- and z-axes of the cross section of the rail, respectively; h_{rt1} denotes the vertical distance between the top surface and torsional center of the cross section of the rail; W_{axle} denotes the axle weight of each vehicle; b_0 denotes half of the transverse distance between the contact points of the wheel and rail; λ denotes the slope of the wheel tread which is a variable depending on the wheel–rail contact position; n_f denotes the total number of the fastener underneath each rail; $\xi_{r,\,p}$ denotes the distance between the pth fastener and the left node of the rail element containing the pth fastener; $\mathbf{N}_{yjh}$ and $\mathbf{N}_{\theta jh}$ of order $1\times\overline{N}_{rr}$ denote, respectively, the time-dependent shape function vectors in the xy plane and in rotation about the x-axis for the rail element, when evaluated at the position of the hth wheelset of the jth vehicle; $\mathbf{N}_{ry,p}$, $\mathbf{N}_{rz,p}$, and $\mathbf{N}_{r\theta,p}$ (p = 1, 2, ..., n_f) denote, respectively, the time-independent shape function vectors in the xy plane, the xz plane, and in rotation about the x-axis for the rail element, when evaluated at the position of the pth fastener.

By omitting the damping of the rail itself, the damping sub-matrix of the rail, $\mathbf{C}_{rr}$, of order $2\overline{N}_r\times 2\overline{N}_r$ can be derived according to the lateral creep between the rails and the wheels of all vehicles (Zhang et al., 2010), the damping of the primary suspension of all vehicles, and the lateral, vertical, and torsional damping of all fasteners.

3.4 Sub-Matrices of Sleeper

The sub-matrices of the sleeper are marked with the subscript "ss". The mass sub-matrix, $\mathbf{M}_{ss}$, stiffness sub-matrix, $\mathbf{K}_{ss}$, and the damping sub-matrix, $\mathbf{C}_{ss}$, of order $\overline{N}_s\times\overline{N}_s$ of all of the sleepers can be written respectively, as

$$\mathbf{M}_{ss}=\mathrm{diag}[\mathbf{M}_{s1}\ \mathbf{M}_{s2}\ \cdots\ \mathbf{M}_{sN_s}] \tag{28}$$

$$\mathbf{K}_{ss}=\mathrm{diag}[\mathbf{K}_{s1}\ \mathbf{K}_{s2}\ \cdots\ \mathbf{K}_{sN_s}] \tag{29}$$

$$\begin{aligned}\mathbf{C}_{ss}&=\mathrm{diag}[\mathbf{C}_{s1}\ \mathbf{C}_{s2}\ \cdots\ \mathbf{C}_{sN_s}]\\ \mathbf{M}_{si}&=\mathrm{diag}[\,m_s\ \ m_s\ \ J_{sx}\,]\\ \mathbf{K}_{si}&=\mathrm{diag}[2k_{rsy}+2k_{sby}\ \ 2k_{rsz}+2k_{sbz}\ \ 2(D_{rr}^2+b_{rt}^2)k_{rsz}+2D_{bal}^2k_{sbz}]\\ \mathbf{C}_{si}&=\mathrm{diag}[2c_{rsy}+2c_{sby}\ \ 2c_{rsz}+2c_{sbz}\ \ 2(D_{rr}^2+b_{rt}^2)c_{rsz}+2D_{bal}^2c_{sbz}]\end{aligned} \tag{30}$$

where m_s and J_{sx} denote the mass and the moment of inertia about x-axis of each sleeper, respectively.

3.5 Sub-Matrices of Bridge and Pier

The sub-matrices of the bridge and pier, marked with the subscripts "bb" and "pp", respectively, can be obtained in a similar way to derivation of the sub-matrices of the rail. It should be noted that the damping property is assumed to be of a Rayleigh type (Yang et al., 2004) in the derivation of the damping sub-matrices of the bridge and pier.

3.6 Sub-Matrices of Train–Rail–Sleeper–Bridge–Pier Interaction

The sub-matrices of train–rail interaction, marked with the subscripts "*tr*" or "*rt*", are induced by the interaction of the wheel and rail, and consist of the train–left rail and train–right rail interaction matrices, which are marked with the subscripts "*tLr*" and "*tRr*", respectively. The stiffness sub-matrices, $\mathbf{K}_{tr}$ and $\mathbf{K}_{rt}$, of order $T_{dof} \times 2N_r$, and the damping sub-matrices, $\mathbf{C}_{tr}$ and $\mathbf{C}_{rt}$, of order $T_{dof} \times 2N_r$, for train–rail interaction can be written respectively, as

$$\mathbf{K}_{tr} = [\mathbf{K}_{tLr}\ \mathbf{K}_{tRr}]_{T_{dof} \times 2N_r} \tag{31}$$

$$\begin{aligned} \mathbf{C}_{tr} &= [\mathbf{C}_{tLr}\ \mathbf{C}_{tRr}]_{T_{dof} \times 2N_r} \\ \mathbf{K}_{rt} &= \mathbf{K}_{tr}^{\mathrm{T}} \\ \mathbf{C}_{rt} &= \mathbf{C}_{tr}^{\mathrm{T}} \end{aligned} \tag{32}$$

where the stiffness matrices, $\mathbf{K}_{tLr}$ and $\mathbf{K}_{tRr}$, and the damping matrices, $\mathbf{C}_{tLr}$ and $\mathbf{C}_{tRr}$, of order $T_{dof} \times 2N_r$ can be expressed respectively, as

$$\mathbf{K}_{tLr} = \sum_{j=1}^{N_v} \sum_{h=1}^{4} \mathbf{K}_{v_j - Lr_h}^{V},$$

$$\mathbf{K}_{tRr} = \sum_{j=1}^{N_v} \sum_{h=1}^{4} \mathbf{K}_{v_j - Rr_h}^{V},$$

$$\mathbf{C}_{tLr} = \sum_{j=1}^{N_v} \sum_{h=1}^{4} \mathbf{C}_{v_j - Lr_h}^{V} + \sum_{j=1}^{N_v} \sum_{h=1}^{4} \mathbf{C}_{v_j - Lr_h}^{L},$$

$$\mathbf{C}_{tRr} = \sum_{j=1}^{N_v} \sum_{h=1}^{4} \mathbf{C}_{v_j - Rr_h}^{V} + \sum_{j=1}^{N_v} \sum_{h=1}^{4} \mathbf{C}_{v_j - Rr_h}^{L},$$

in which $\mathbf{K}_{v_j - Lr_h}^{V}$ and $\mathbf{K}_{v_j - Rr_h}^{V}$ represent, respectively, the stiffness matrices induced by the vertical interaction between the *h*th wheelset of the *j*th vehicle and the left and right rails; $\mathbf{C}_{v_j - Lr_h}^{V}$ and $\mathbf{C}_{v_j - Rr_h}^{V}$ represent, respectively, the damping matrices induced by the vertical interaction between the *h*th wheelset of the *j*th vehicle and the left and right rails; and $\mathbf{C}_{v_j - Lr_h}^{L}$ $\mathbf{C}_{v_j - Rr_h}^{L}$ represent, respectively, the damping matrices induced by the lateral creepage between the *h*th wheelset of the *j*th vehicle and the left and right rails (Zhang et al., 2010; Kalker, 1967).

The sub-matrices of rail–sleeper interaction, marked with the subscripts "*rs*" or "*sr*", are induced by the stiffness and damping of all fasteners between the rail and sleeper. The sub-matrices of sleeper–bridge interaction, marked with the subscripts "*sb*" or "*bs*", are induced by the stiffness and damping of all ballasts between the sleeper and bridge. In addition, the sub-matrices of bridge–pier interaction, marked with the subscripts "*bp*" or "*pb*", are induced by the stiffness and damping of all bearings between the bridge and pier. To reduce repetitions, the deviations of all sub-matrices for rail–sleeper–bridge–pier interaction are not listed here, but can be calculated according to equations (1) to (32).

3.7 Load Sub-Vectors of Train, Rail, Sleeper, Bridge, and Pier

The load sub-vector of the train, $\mathbf{F}_t$, of order $T_{dof} \times 1$ can be written as

$$\begin{aligned}\mathbf{F}_t &= \mathbf{F}_t^1 + \mathbf{F}_t^2 \\ \mathbf{F}_t^1 &= [\mathbf{F}_{v1}^1 \ \ \mathbf{F}_{v2}^1 \ \ \cdots \ \ \mathbf{F}_{vN_v}^1]^{\mathbf{T}} \\ \mathbf{F}_t^2 &= [\mathbf{F}_{v1}^2 \ \ \mathbf{F}_{v2}^2 \ \ \cdots \ \ \mathbf{F}_{vN_v}^2]^{\mathbf{T}}\end{aligned} \tag{33}$$

The load vector of the jth vehicle, $\mathbf{F}_{vj}^1$ and $\mathbf{F}_{vj}^2$, of order 23×1 can be written respectively, as

$$\mathbf{F}_{vj}^1 = \begin{Bmatrix} 0 \\ 0 \\ 0 \\ 0 \\ 0 \\ 0 \\ k_{pz}[2r(x_{j1}^V) + 2r(x_{j2}^V)] \\ k_{pz}b_2[r(x_{j1}^C) + r(x_{j2}^C)] \\ k_{pz}L_t[2r(x_{j1}^V) - 2r(x_{j2}^V)] \\ 0 \\ 0 \\ k_{pz}[2r(x_{j3}^V) + 2r(x_{j4}^V)] \\ k_{pz}b_2[r(x_{j3}^C) + r(x_{j4}^C)] \\ k_{pz}L_t[2r(x_{j3}^V) - 2r(x_{j4}^V)] \\ 0 \\ \frac{W_{axle}\lambda}{b_0}r(x_{j1}^A) \\ 0 \\ \frac{W_{axle}\lambda}{b_0}r(x_{j2}^A) \\ 0 \\ \frac{W_{axle}\lambda}{b_0}r(x_{j3}^A) \\ 0 \\ \frac{W_{axle}\lambda}{b_0}r(x_{j4}^A) \\ 0 \end{Bmatrix}^{\mathbf{T}}$$

$$\mathbf{F}_{vj}^2 = \begin{Bmatrix} 0 \\ 0 \\ 0 \\ 0 \\ 0 \\ 0 \\ c_{pz}[2\dot{r}(x_{j1}^V) + 2\dot{r}(x_{j2}^V)] \\ c_{pz}b_2[\dot{r}(x_{j1}^C) + \dot{r}(x_{j2}^C)] \\ c_{pz}L_t[2\dot{r}(x_{j1}^V) - 2\dot{r}(x_{j2}^V)] \\ 0 \\ 0 \\ c_{pz}[2\dot{r}(x_{j3}^V) + 2\dot{r}(x_{j4}^V)] \\ c_{pz}b_2[\dot{r}(x_{j3}^C) + \dot{r}(x_{j4}^C)] \\ c_{pz}L_t[2\dot{r}(x_{j3}^V) - 2\dot{r}(x_{j4}^V)] \\ 0 \\ f_{Lj1}^{22}[\dot{r}(x_{j1}^A) + \frac{1}{2}\dot{r}(x_{j1}^G)] + f_{Rj1}^{22}[\dot{r}(x_{j1}^A) - \frac{1}{2}\dot{r}(x_{j1}^G)] \\ 0 \\ f_{Lj2}^{22}[\dot{r}(x_{j2}^A) + \frac{1}{2}\dot{r}(x_{j2}^G)] + f_{Rj2}^{22}[\dot{r}(x_{j2}^A) - \dot{r}(x_{j2}^G)] \\ 0 \\ f_{Lj3}^{22}[\dot{r}(x_{j3}^A) + \frac{1}{2}\dot{r}(x_{j3}^G)] + f_{Rj3}^{22}[\dot{r}(x_{j3}^A) - \frac{1}{2}\dot{r}(x_{j3}^G)] \\ 0 \\ f_{Lj4}^{22}[\dot{r}(x_{j4}^A) + \frac{1}{2}\dot{r}(x_{j4}^G)] + f_{Rj4}^{22}[\dot{r}(x_{j4}^A) - \frac{1}{2}\dot{r}(x_{j4}^G)] \\ 0 \end{Bmatrix}^{\mathbf{T}},$$

where $r(x_{jh}^V)$, $r(x_{jh}^C)$, $r(x_{jh}^A)$, and $r(x_{jh}^G)$ denote the track elevation, cross level, alignment, and gauge irregularities, respectively, at the hth wheel–rail contact point of the jth vehicle; $\dot{r}(\cdot)$ denotes the first derivative of track irregularity; b_2 denotes half of the transverse distance between the vertical primary suspension system and L_t denotes half of the bogie axle base; f_{Ljh}^{22} denotes the lateral creep coefficient between the left rail and the hth (h = 1–4) wheelset of the jth vehicle, and f_{Rjh}^{22} denotes the lateral creep coefficient between the right rail and the corresponding wheelset.

The load sub-vector of the rail, $\mathbf{F}_r$, of order $2N_r\times1$ can be written as

$$\begin{aligned}\mathbf{F}_r &= \begin{bmatrix}\mathbf{F}_r^L \\ \mathbf{F}_r^R\end{bmatrix} \\ \mathbf{F}_r^L &= \mathbf{F}_r^{L0} + \mathbf{F}_r^{L1} + \mathbf{F}_r^{L2} + \mathbf{F}_r^{L3} + \mathbf{F}_r^{L4} + \mathbf{F}_r^{L5} + \mathbf{F}_r^{L6} + \mathbf{F}_r^{L7} + \mathbf{F}_r^{L8} + \mathbf{F}_r^{L9} + \mathbf{F}_r^{L10} \\ \mathbf{F}_r^R &= \mathbf{F}_r^{R0} + \mathbf{F}_r^{R1} + \mathbf{F}_r^{R2} + \mathbf{F}_r^{R3} + \mathbf{F}_r^{R4} + \mathbf{F}_r^{R5} + \mathbf{F}_r^{R6} + \mathbf{F}_r^{R7} + \mathbf{F}_r^{R8} + \mathbf{F}_r^{R9} + \mathbf{F}_r^{R10}\end{aligned} \tag{34}$$

where $\mathbf{F}_r^{L0}$, $\mathbf{F}_r^{L1}$, $\mathbf{F}_r^{L2}$, $\mathbf{F}_r^{L3}$, and $\mathbf{F}_r^{L4}$ of order $N_r\times1$ represent the load vectors of each wheelset acting on the left rail caused by the train's weight, the track elevation irregularity, the cross level irregularity, the alignment irregularity, and the gauge irregularity, respectively; $\mathbf{F}_r^{L5}$, $\mathbf{F}_r^{L6}$, $\mathbf{F}_r^{L7}$, and $\mathbf{F}_r^{L8}$ of order $N_r\times1$ represent the load vectors of each wheelset acting on the left rail caused by the velocities of the track elevation, cross level, alignment, and gauge irregularities, respectively; and $\mathbf{F}_r^{L9}$ $\mathbf{F}_r^{L10}$ of order $N_r\times1$ represent the load vectors of each wheelset acting on the left rail that are caused by

accelerations in the track elevation and cross level irregularities, respectively; and $\mathbf{F}_r^{R0}$ to $\mathbf{F}_r^{R10}$ similarly represent the load vectors of each wheelset acting on the right rail.

Each of the elements of the load sub-vector of the sleeper, $\mathbf{F}_s$, of order $\overline{N}_s \times 1$, the load sub-vector of the bridge, $\mathbf{F}_b$, of order $\overline{N}_b \times 1$, and the load sub-vector of the pier, $\mathbf{F}_p$, of order $\overline{N}_p \times 1$ are zero.

4 NUMERICAL VERIFICATION

To verify the theory presented in this paper, the vertical dynamic responses of a TTBI system, which were obtained using the proposed 3D rail–bridge coupling element (3D element) and the 2D rail–bridge coupling element presented by Lou et al. (2012) (2D element), respectively, are used. A train consisting of five identical vehicles is considered to run over a single–track bridge along the centerline of the bridge, with no consideration made for torsional action. The railway track is assumed to be smooth and continuous throughout and has a total length of 100 m and LRE = 0.625 m. The central part of the railway track is supported on a 3-span continuous bridge with spans of 20 m and LBE = 5.0 m, while the left and right parts of track are supported on embankments, both with lengths of 20 m. The vertical parameters of vehicle, track, and bridge can be found in Lou et al. (2012), the spatial parameters of the identical vehicle can be found in Yang et al. (2004), and the spatial parameters of the identical track and bridge are listed in Table 1. To solve the equation of motion for the TTBI system, the Wilson-ϑ method is used with $\vartheta = 1.4$ and a moving length of the vehicles of 0.1 m along the track for each time step. The analysis is performed by applying the train speeds from 25 m/s to 200 m/s at 25 m/s intervals. The vertical dynamic responses of bridge, sleeper, rail, and vehicle obtained by the 3D element and the 2D element at various train speeds are shown in Table 2, where the term "Carbody acceleration" means the maximum vertical acceleration at the centroid of the last carbody, "Rail displacement" means the maximum vertical displacement of the rail at the middle of the central span, "Sleeper displacement" means the maximum vertical displacement of the sleeper immediately to the right of the middle of the central span, and "Bridge displacement" means the maximum vertical displacement of the bridge at the middle of central span. It can be observed from Table 2 that there are only minimal differences between the solutions obtained using the 3D element and those using the 2D element, where the differences of the displacements of bridge, sleeper, and rail are less than 1.00%, and the differences between the carbody acceleration at various train speeds are not larger than 4.00%. This thus confirms the accuracy of the proposed 3D rail–bridge coupling element in simulating the dynamic responses of a TTBI system.

Train speed (m/s)		25	50	75	100	125	150	175	200
Bridge displacement (mm)	3D element	0.165	0.181	0.176	0.196	0.205	0.503	0.517	0.411
	2D element	0.166	0.181	0.176	0.195	0.204	0.501	0.515	0.410
Sleeper displacement (mm)	3D element	0.268	0.289	0.305	0.327	0.342	0.600	0.652	0.559
	2D element	0.270	0.290	0.304	0.325	0.339	0.598	0.649	0.556
Rail displacement (mm)	3D element	0.725	0.730	0.734	0.750	0.774	1.062	1.120	0.997
	2D element	0.729	0.733	0.732	0.747	0.769	1.056	1.116	0.992
Carbody acceleration (m/s^2)	3D element	0.008	0.015	0.021	0.025	0.029	0.043	0.041	0.055
	2D element	0.008	0.015	0.021	0.026	0.030	0.044	0.042	0.053

Table 2: Comparsion of vertical dynamic responses of TTBI system at various train speeds.

5 ILLUSTRATIVE EXAMPLES

5.1 Parameters of a TTBI System

The proposed 3D rail–bridge coupling element is applied in the following three examples. The first example is shown in relation to an investigation of the influence of the efficiency and accuracy of LRE and LBE on the spatial dynamic responses of a TTBI system. The other two examples are shown in relation to an investigation of the effects of two types of track models and two types of wheel–rail interaction models on the spatial dynamic responses of a TTBI system, respectively. A seven-span continuous beam bridge, with a span length of 40 m + 5 × 60 m + 40 m = 380 m, is considered. The heights of the piers are 20 m, and the length of the pier element (LPE) is 2.5 m. However, to save the length of the paper, the influence of LPE is not considered in this paper. The parameters of the track and bridge already listed in Table 1 are adopted unless otherwise stated. A train consisting of five identical vehicles is considered to move over the bridge from left to right, and the major parameters of each vehicle are listed in Table 3. The PSDs of a German high-speed track spectrum of low irregularity (Zhai and Xia, 2011) are adopted, i.e.,

track elevation irregularity: $\mathbf{S}_{rr}^{V}(\Omega)=\dfrac{A_V\Omega_c^2}{(\Omega^2+\Omega_r^2)(\Omega^2+\Omega_c^2)}$,

track alignment irregularity: $\mathbf{S}_{rr}^{A}(\Omega)=\dfrac{A_A\Omega_c^2}{(\Omega^2+\Omega_r^2)(\Omega^2+\Omega_c^2)}$,

track cross level irregularity: $\mathbf{S}_{rr}^{C}(\Omega)=\dfrac{A_V/b_0^2\Omega_c^2\Omega^2}{(\Omega^2+\Omega_r^2)(\Omega^2+\Omega_c^2)(\Omega^2+\Omega_s^2)}$,

and track gauge irregularity: $\mathbf{S}_{rr}^{G}(\Omega)=\dfrac{A_G\Omega_c^2\Omega^2}{(\Omega^2+\Omega_r^2)(\Omega^2+\Omega_c^2)(\Omega^2+\Omega_s^2)}$,

where $\Omega = 2\pi/\lambda_r$ denotes the spatial frequency (rad/m), λ_r denotes the wavelength of the irregularity (m), $\Omega_c = 0.8246$ rad/m, $\Omega_r = 0.0206$ rad/m, $\Omega_s = 0.438$ rad/m, $A_V = 4.032 \times 10^{-7}$ m·rad, $A_A = 2.119 \times 10^{-7}$ m·rad, and $A_G = 0.532 \times 10^{-7}$ m·rad.

Notation	Value	Notation	Value	Notation	Value
m_c (kg)	4.4E4	I_{wz} (kg·m^2)	1.1E3	c_{py} (N·s/m)	0.0
m_t (kg)	2.4E3	k_{sx} (N/m)	2.8E5	c_{pz} (N·s/m)	5.0E4
m_w (kg)	2.4E3	k_{sy} (N/m)	2.8E5	h_1 (m)	1.14
W_{axle} (kg)	1.46E4	k_{sz} (N/m)	3.0E5	h_2 (m)	−0.14
I_{cx} (kg·m^2)	1.0E5	k_{px} (N/m)	1.5E7	h_3 (m)	0.24
I_{cy} (kg·m^2)	2.7E6	k_{py} (N/m)	5.0E6	b_0 (m)	0.75
I_{cz} (kg·m^2)	2.7E6	k_{pz} (N/m)	7.0E5	b_1 (m	0.95
I_{tx} (kg·m^2)	1.8E3	c_{sx} (N·s/m)	1.0E6	b_2 (m)	1.0
I_{ty} (kg·m^2)	2.2E3	c_{sy} (N·s/m)	2.5E4	L_c (m)	8.6875
I_{tz} (kg·m^2)	2.2E3	c_{sz} (N·s/m)	6.0E4	L_t (m)	1.25
I_{wx} (kg·m^2)	1.1E3	c_{px} (N·s/m)	0.0	R_0 (m)	0.4575

Table 3: Major parameters of vehicle.

The time domain samples of track irregularities with 1 m $\leq \lambda_r \leq$ 120 m are simulated using the method proposed by Zhai and Xia (2011), and an analysis is performed by applying train speeds between 2.78 m/s and 97.2 m/s at 2.78 m/s intervals; that is, from 10 km/h to 350 km/h at 10 km/h intervals.

5.2 Example 1: Influence of the Efficiency and Accuracy of LRE and LBE on the Dynamic Responses of the TTBI System

To illustrate the efficiency and accuracy of the proposed 3D rail–bridge coupling element, the following six cases are studied, as shown in Table 4. The rail–bridge coupling element with LRE = LBE is used in Cases 1-1 to 1-5, while the proposed element is adopted in Case 1-6. The spatial dynamic responses of the TTBI system for Cases 1-1 to 1-6 at various train speeds are plotted in Figures 6 to 19 and the calculation time and differences, D_{e1}, for Cases 1-1 to 1-6 at a train speed of 350 km/h are shown in Table 5. Herein, the differences, D_{e1}, between the dynamic responses of different calculation cases is defined as $D_{e1} = (D_{yn11}-D_{yn12})/D_{yn11} \times 100\%$, where D_{yn11} and D_{yn12} denote the dynamic responses obtained by the proposed element (Case 1-6) and the rail–bridge coupling element of equal length (Cases 1-1 to 1-5), respectively. For convenience hereafter, the "bridge midpoint" means the midpoint of the fourth span for the seven-span bridge; "sleeper", "rail" and "fastener" mean the sleeper, left rail and left fastener immediately on the bridge midpoint, respectively; "carbody" and "bogie" mean the carbody and front bogie of the third vehicle, respectively; and the "derailment factor" and "offload factor" mean the derailment factor and offload factor of the left wheel for the second wheelset of the third vehicle, respectively. The derailment factor is defined as the ratio of the lateral wheel–rail force to the vertical wheel–rail force of the same wheel, while the offload factor is defined as the ratio of the offload in the vertical wheel–rail force to the static vertical wheel–rail force of the same wheel (Xia et al., 2006). Figures 6 and 7 show the maximum lateral and vertical accelerations of the bridge midpoint, respectively; Figures 8 and 9 show the maximum lateral and vertical accelerations of the sleeper, respectively; Figures 10 and 11 show the maximum lateral and vertical accelerations of the left rail, respectively; Figures 12 and 13 show the maximum lateral and vertical accelerations of the carbody, respectively; Figures 14 and 15 show the maximum lateral and vertical accelerations of the bogie, respectively; Figures 16 and 17 show the maximum lateral force and vertical pressure of the left fastener, respectively; and Figures 18 and 19 plot the maximum derailment factor and offload factor, respectively. As is shown, the differences in the dynamic responses between Cases 1-1 to 1-5 appear to decrease as the lengths of the elements are reduced, indicating that the use of a shorter length of element tends to greatly improve the calculation accuracy. However, the corresponding calculation time increases significantly in relation to an increase in the number of DOFs. When the LBE is shorter than 2.5 m (Cases 1-3 to 1-5), the differences in the accelerations of the bridge midpoint (Figures 6 and 7) are much smaller than those of the accelerations of the sleeper (Figures 8 and 9), of the accelerations of the rail (Figures 10 and 11), of the fastener forces (Figures 16 and 17), and of the wheel–rail interactions (Figures 18 and 19), due to the fact that the mass and stiffness of the bridge are much larger than those of sleeper and rail. For instance, the ratios of lateral and vertical flexural rigidity of the bridge to those of the single rail are respectively 4.28×10^6 and 9.99×10^4. Similar phenomenon can also be observed for the lateral and vertical accelerations of the carbody (Figures 12 and

13) and for the lateral acceleration of the bogie (Figure 14), because the vehicle's suspension systems and wheel–rail creepage serve to some extent as an energy dissipating mechanism. It is evident that a sufficiently fine mesh, i.e., LRE = l_{sp}, should be adopted for the rail if accurate accelerations of sleeper and rail, fastener forces, and wheel–rail interactions are required. By comparing the dynamic responses of Case 1-2 with those of Case 1-6, it can be seen that the influence of LRE on the bridge dynamic responses is also important if the track irregularities are considered, which is different from the case that considers an ideal smooth track (Lou et al., 2010). As shown in Table 4, the major difference between the two calculation cases in modeling rail–bridge interaction is that Case 1-2 uses the rail–bridge coupling element with LBE = LRE = 5.0 m, while Case 1-6 uses the proposed element with LBE = 5.0 and LRE = 0.625 m. Although LBE in Case 1-2 is equal to that in Case 1-6, the differences in the lateral and vertical accelerations of the bridge at a train speed of 350 km/h may reach 8.87% and 13.90%, respectively. It is interesting to note that negligible differences between the bridge, sleeper, rail, and the vehicle dynamic responses can be observed in Cases 1-5 and 1-6. As shown in Table 4, the major differences between the two calculation cases in modeling rail–bridge interaction is that Case 1-5 uses the rail–bridge coupling element with LBE = LRE = 0.625 m, while Case 1-6 uses the proposed element with LBE = 5.0 and LRE = 0.625 m. Although LBE in Case 1-6 is eight times that in Case 1-5, an excellent agreement of the dynamic responses can be obtained because of the high flexural rigidity of bridge. Furthermore, the proposed element helps to save calculation time compared with the rail–bridge coupling element of equal length, due to the reduction of DOFs. For example, the total CPU times for Case 1-5 and Case 1-6 are 1248.2 s and 902.4 s on a 2.8 GHz personal computer, respectively, and the ratio of the latter to the former is 0.723. Therefore, it is concluded that the proposed 3D rail–bridge coupling element with shorter rail elements and longer bridge elements can not only help to save calculation time but can also provide satisfactory results when investigating the spatial dynamic responses of a TTBI system.

Calculation case	LBE (m)	LRE (m)	LPE (m)	Number of DOFs
Case 1-1	10.0	10.0	2.5	2628
Case 1-2	5.0	5.0		3198
Case 1-3	2.5	2.5		4338
Case 1-4	1.25	1.25		6618
Case 1-5	0.625	0.625		11178
Case 1-6	5.0	0.625		8518

Table 4: Calculation cases.

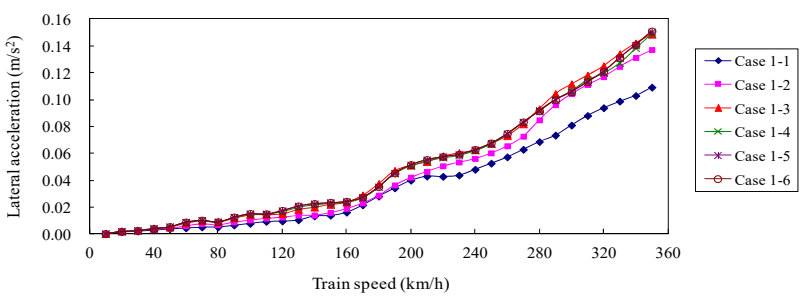

Figure 6: Maximum lateral acceleration of bridge midpoint with respect to train speed.

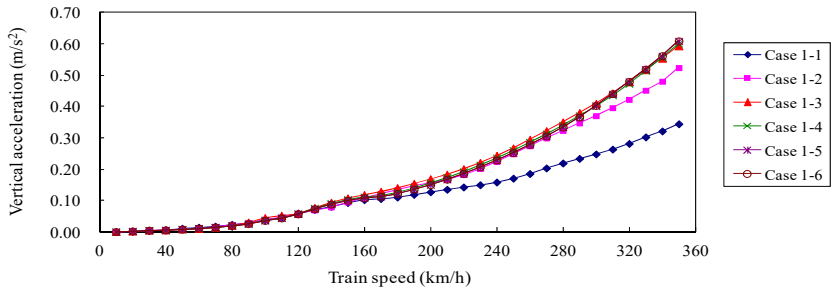

Figure 7: Maximum vertical acceleration of bridge midpoint with respect to train speed.

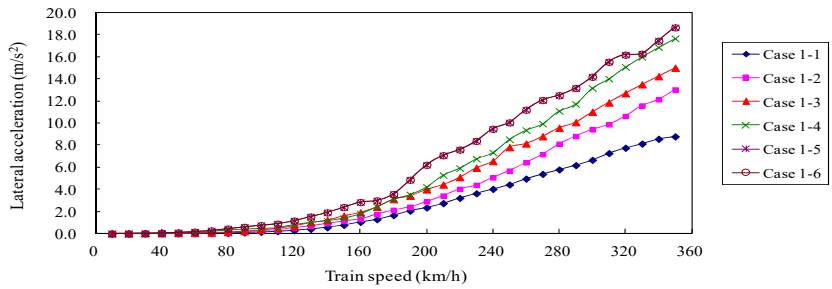

Figure 8: Maximum lateral acceleration of sleeper with respect to train speed.

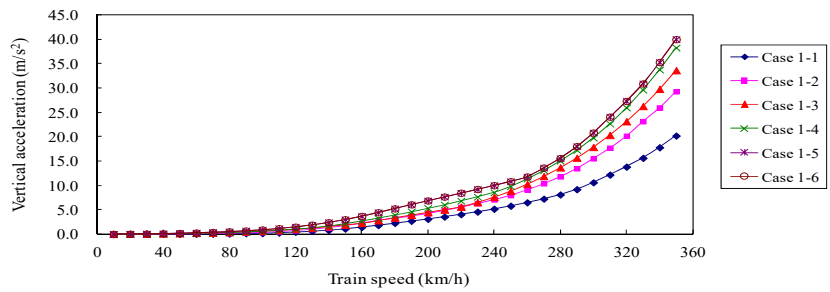

Figure 9: Maximum vertical acceleration of sleeper with respect to train speed.

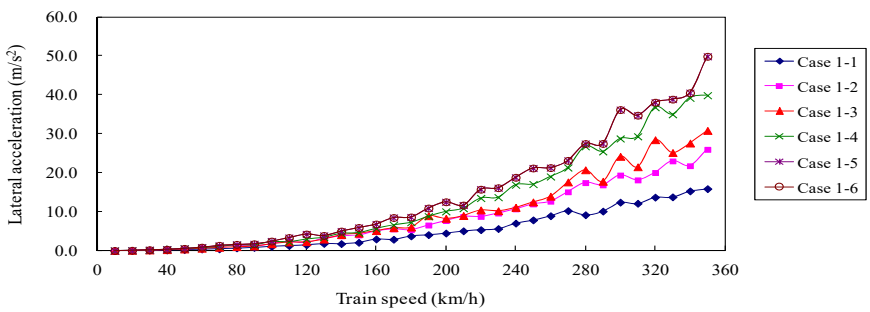

Figure 10: Maximum lateral acceleration of rail with respect to train speed.

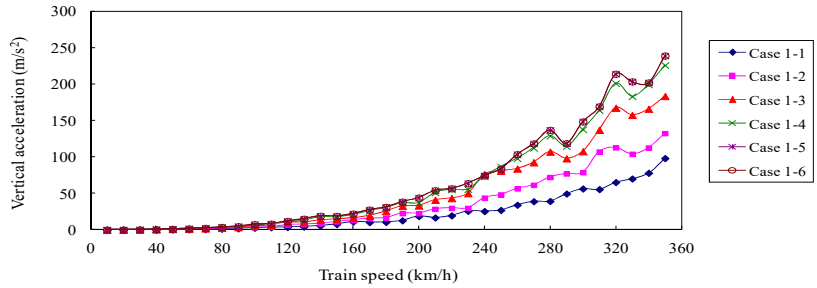

Figure 11: Maximum vertical acceleration of rail with respect to train speed.

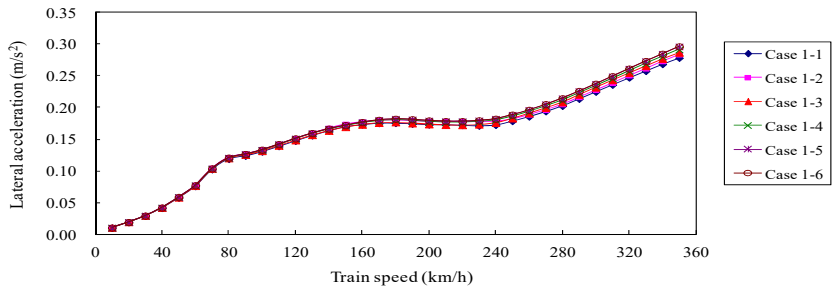

Figure 12: Maximum lateral acceleration at centroid of carbody with respect to train speed.

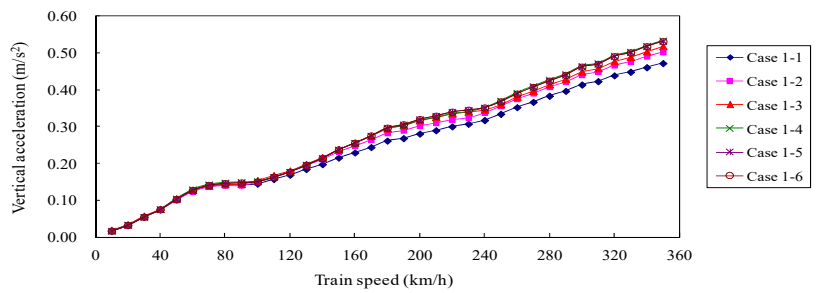

Figure 13: Maximum vertical acceleration at centroid of carbody with respect to train speed.

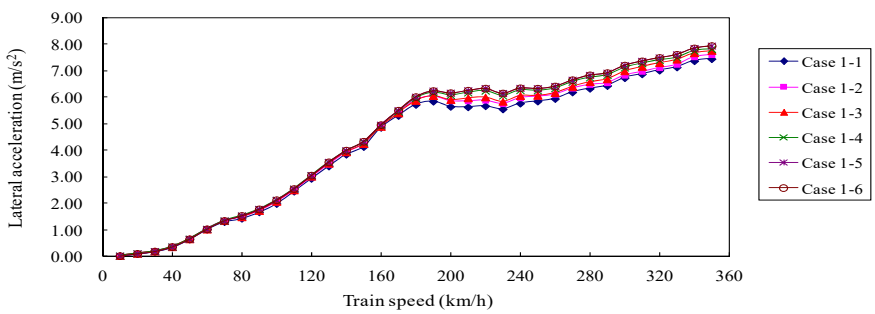

Figure 14: Maximum lateral acceleration at centroid of bogie with respect to train speed.

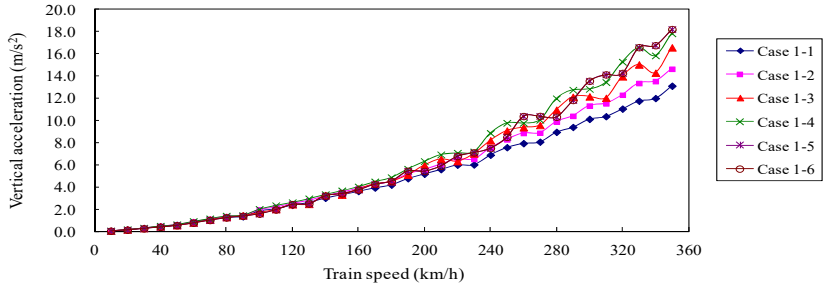

Figure 15: Maximum vertical acceleration at centroid of bogie with respect to train speed.

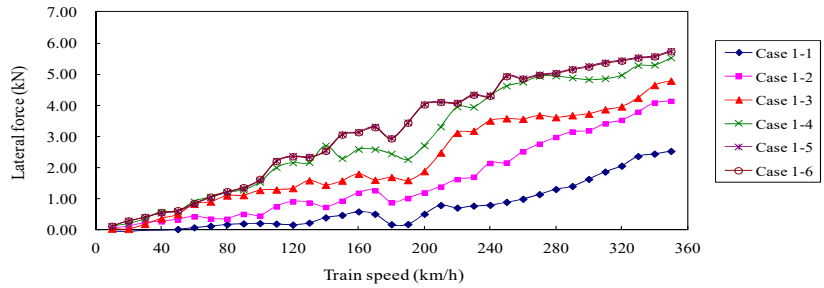

Figure 16: Maximum lateral force of fastener with respect to train speed.

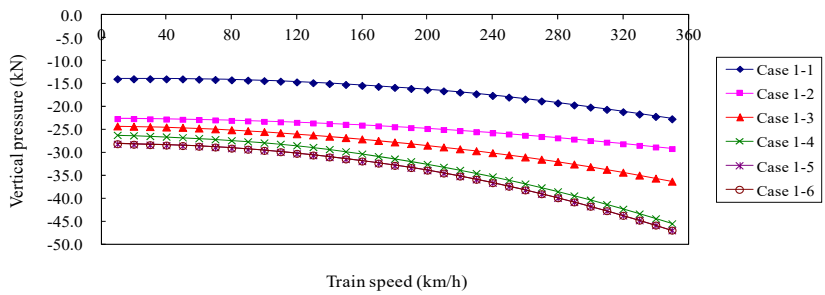

Figure 17: Maximum vertical pressure of fastener with respect to train speed.

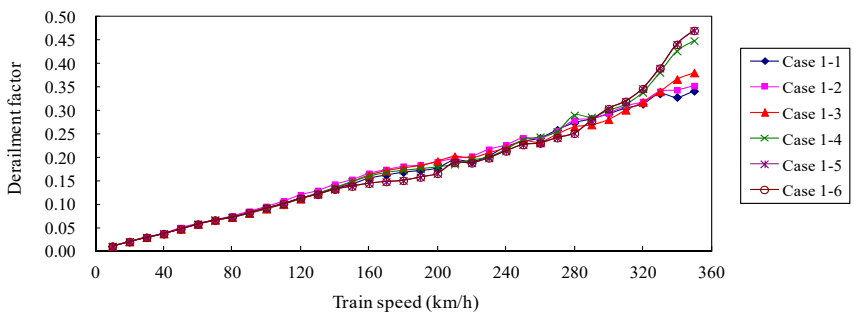

Figure 18: Maximum derailment factor with respect to train speed.

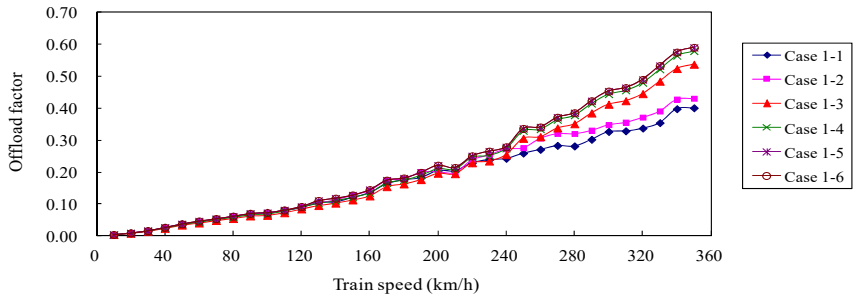

Figure 19: Maximum offload factor with respect to train speed.

Calculation case	Case 1-1	Case 1-2	Case 1-3	Case 1-4	Case 1-5	Case 1-6
Calculation time (s)	303.4	358.7	475.9	711.9	1248.2	902.4
D_{e1} of bridge midpoint lateral acceleration (%)	27.45	8.87	1.22	1.03	0.29	0.00
D_{e1} of bridge midpoint vertical acceleration (%)	43.41	13.90	2.56	1.31	0.09	0.00
D_{e1} of sleeper lateral acceleration (%)	52.91	30.15	19.60	5.31	−0.01	0.00
D_{e1} of sleeper vertical acceleration (%)	49.55	26.74	15.96	4.29	−0.01	0.00
D_{e1} of rail lateral acceleration (%)	68.14	47.92	34.20	20.05	−0.01	0.00
D_{e1} of rail vertical acceleration (%)	58.88	44.53	23.26	5.47	−0.01	0.00
D_{e1} of carbody lateral acceleration (%)	6.03	4.17	3.25	1.61	0.00	0.00
D_{e1} of carbody vertical acceleration (%)	11.19	5.53	2.49	0.45	0.00	0.00
D_{e1} of bogie lateral acceleration (%)	6.22	4.22	2.30	1.60	−0.01	0.00
D_{e1} of bogie vertical acceleration (%)	28.00	19.63	9.06	2.05	0.01	0.00
D_{e1} of lateral force of fastener (%)	55.92	27.96	16.67	3.77	−0.26	0.00
D_{e1} of vertical pressure of fastener (%)	51.72	37.90	22.75	3.15	−0.04	0.00
D_{e1} of derailment factor (%)	27.40	25.00	19.09	4.60	0.00	0.00
D_{e1} of offload factor (%)	32.04	26.99	8.92	1.84	0.01	0.00

Table 5: Calculation time and accuracy for different calculation cases at train speed of 350 km/h.

5.3 Example 2: Influence of Two Types of Track Models on Dynamic Responses of TTBI System

In this example, two types of track models are considered, with the same train, bridge, and track irregularity as presented in Section 5.1. One is a double-layer track model which has the same sleepers that were considered in Section 5.1, while the other is a single-layer track model in which the sleepers are ignored. The parameters LBE = 5.0 m and LRE = 0.625 m are adopted in both models. The lateral and vertical stiffnesses, k_{rby} and k_{rbz}, of the discrete springs between the rail and bridge in the single-layer track model can be obtained by considering k_{rsy} and k_{sby}, k_{rsz} and k_{sbz}, respectively, in series in the double-layer track model with sleepers ignored, i.e., $k_{rby} = k_{rsy} \cdot k_{sby}/(k_{rsy} + k_{sby})$ and $k_{rbz} = k_{rsz} \cdot k_{sbz}/(k_{rsz} + k_{sbz})$. Similarly, the lateral and vertical damping coefficients, c_{rby} and c_{rbz}, of the discrete dampers between the rail and bridge in the single-layer track model can be obtained as $c_{rby} = c_{rsy} \cdot c_{sby}/(c_{rsy} + c_{sby})$ and $c_{rbz} = c_{rsz} \cdot c_{sbz}/(c_{rsz} + c_{sbz})$. To investigate the influence of the mass, m_s, of the sleeper on the spatial dynamic responses of the TTBI system, five masses of 170 kg, 255 kg, 340 kg, 425 kg, and 510 kg are applied, which are equal to 0.50, 0.75, 1.00, 1.25, and

1.50 times the normal value, respectively. The other parameters are the same as those in Table 1. It is of note that the mass of the sleeper is added to the dead load of the bridge in the single-layer track model, but that a detailed derivation of the stiffness and damping matrices of the rail–bridge interaction is not given here. However, it can be obtained by following a procedure similar to that given in Sections 2.2 and 2.3. To investigate the influence of the track model on the spatial dynamic responses of the TTBI system, the difference, D_{e2}, between the dynamic responses based on the single-layer track model and those based on the double-layer track model can be defined as $D_{e2} = (D_{yn21}–D_{yn22})/D_{yn21} \times 100\%$, where D_{yn21} and D_{yn22} denote the dynamic responses obtained by the single-layer track model and by the double-layer track model, respectively. The differences, D_{e2}, of the dynamic responses of the TTBI system at various train speeds based on the single-layer track model and the double-layer track model with $m_s = 170$ kg, $m_s = 225$ kg, $m_s = 340$ kg, $m_s = 425$ kg, and $m_s = 510$ kg, are plotted in Figures 20 to 27. Figures 20 and 21 show the differences in the maximum lateral and vertical accelerations of the bridge midpoint, respectively; Figures 22 and 23 show the differences in the maximum lateral and vertical accelerations of the rail, respectively; Figures 24 and 25 show the differences in the maximum lateral and vertical accelerations of the carbody, respectively; and Figures 26 and 27 plot the differences in the maximum derailment factor and offload factor, respectively. Differences in the dynamic responses based on the single-layer and double-layer track models can be seen in Figures 20 to 27, and it is evident that the differences in both the maximum lateral and vertical dynamic responses generally increase with an increase in the mass of sleeper and train speed. Although the differences in the maximum lateral and vertical acceleration of the carbody (Figures 24 and 25) are negligibly small ($\leq 2\%$), due to the energy dissipating effect of the vehicle's suspension systems and wheel–rail creepage, the differences in other dynamic responses are quite visible, particularly at higher train speeds. For instance, the differences in lateral acceleration of the bridge (Figure 20), lateral acceleration of the rail (Figure 22), and the derailment factor (Figure 26) are larger than 100%, 10%, and 4%, respectively, in the present calculation cases. Figures 28 to 31 plot the maximum lateral and vertical accelerations of the bridge midpoint and rail with the single-layer track model and double-layer track model with $m_s = 170$ kg, $m_s = 255$ kg, $m_s = 340$ kg, $m_s = 425$ kg, and $m_s = 510$ kg, respectively. As can be seen from Figures 28 to 31, the lateral and vertical accelerations of the bridge midpoint tend to increase steadily with an increase in the mass of the sleeper, while the lateral and vertical accelerations of the rail show a trend of slight decrease at higher train speeds. This can be explained by the fact that the sleepers serve as a medium for transmitting the kinetic energy brought by the moving train from the rail to the bridge. The increase in the mass of the sleeper thus increases the train-induced impact effect on the bridge, while reducing the vibration amplitude of the rail. In addition, the two-layer track model allows us to compute not only the bridge responses, rail responses, vehicle responses, and wheel–rail interaction, but also the sleeper responses and the fastener force. However, it is worth noting that the single-layer track model saves calculation time because of the reduction of DOFs. For example, the DOFs of the single-layer and double-layer track models are 6691 and 8518 respectively, while the corresponding calculation times are 720.1 s and 902.4 s on a 2.8 GHz personal computer, respectively. It is thus concluded that the double-layer model, although more time consuming, is shown to be more accurate.

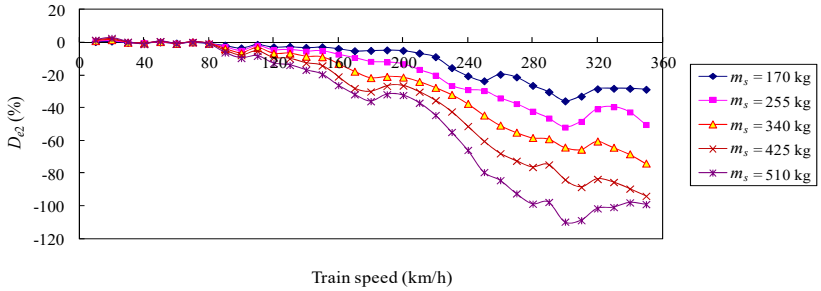

Figure 20: Differences, D_{e2}, in maximum lateral acceleration of the bridge midpoint with respect to train speed.

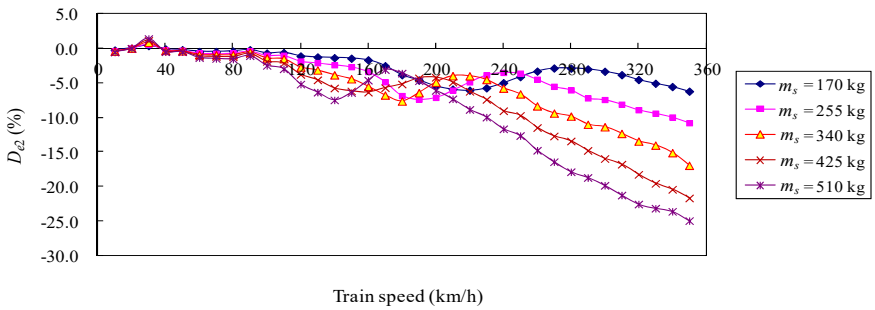

Figure 21: Differences, D_{e2}, in maximum vertical acceleration of bridge midpoint with respect to train speed.

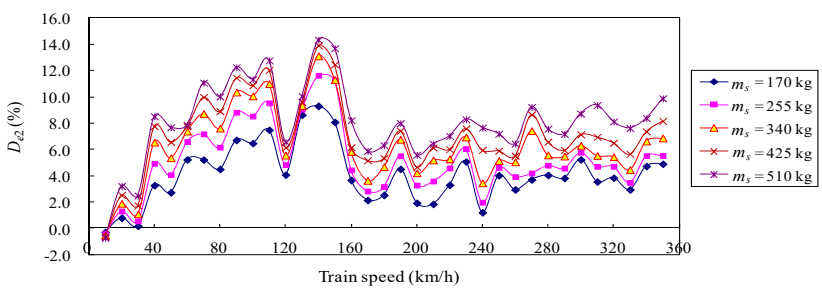

Figure 22: Differences, D_{e2}, in maximum lateral acceleration of rail with respect to train speed.

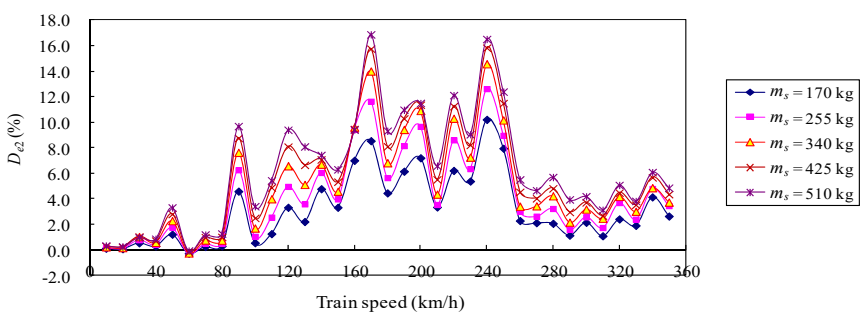

Figure 23: Differences, D_{e2}, in maximum vertical acceleration of rail with respect to train speed.

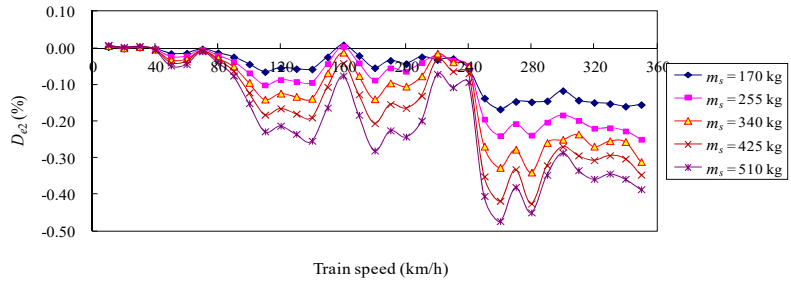

Figure 24: Differences, D_{e2}, in maximum lateral acceleration at centroid of carbody with respect to train speed.

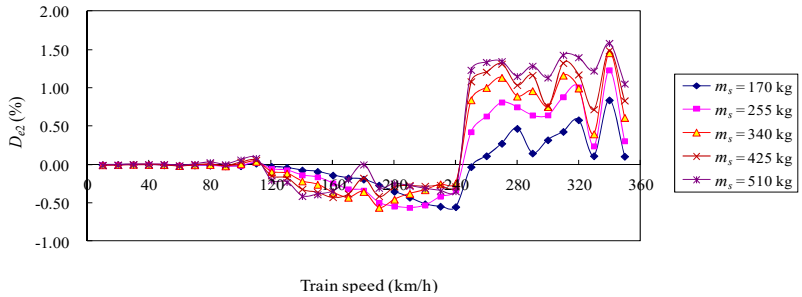

Figure 25: Differences, D_{e2}, in maximum vertical acceleration at centroid of carbody with respect to train speed.

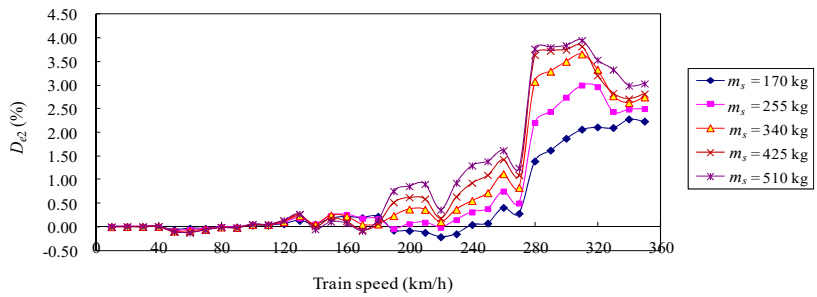

Figure 26: Differences, D_{e2}, in maximum derailment factor with respect to train speed.

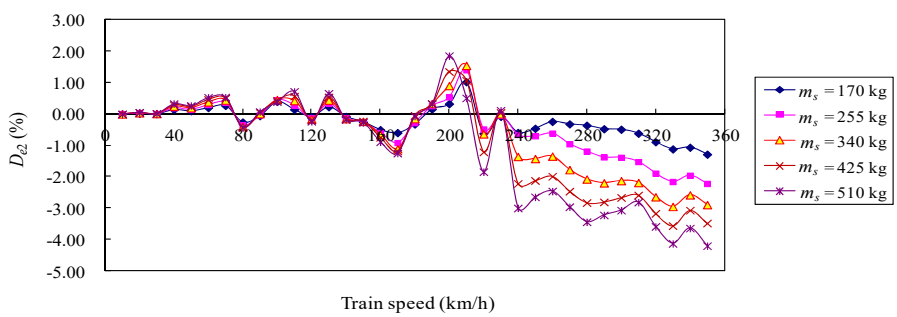

Figure 27: Differences, D_{e2}, in maximum offload factor with respect to train speed.

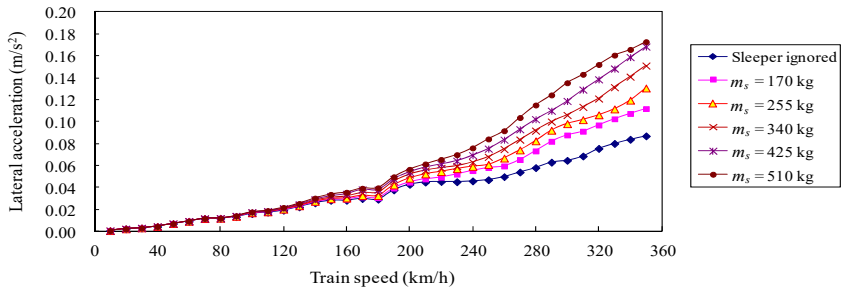

Figure 28: Maximum lateral acceleration of bridge midpoint with respect to train speed.

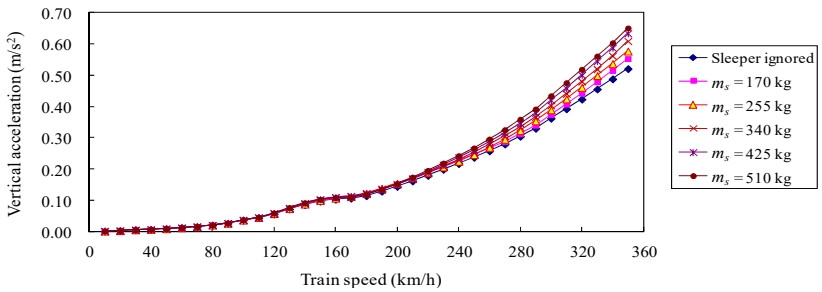

Figure 29: Maximum vertical acceleration of bridge midpoint with respect to train speed.

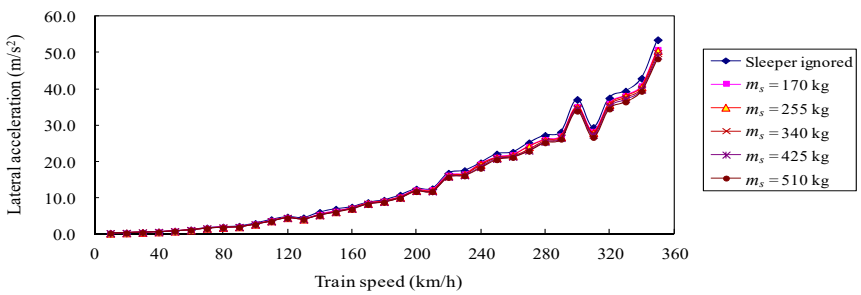

Figure 30: Maximum lateral acceleration of rail with respect to train speed.

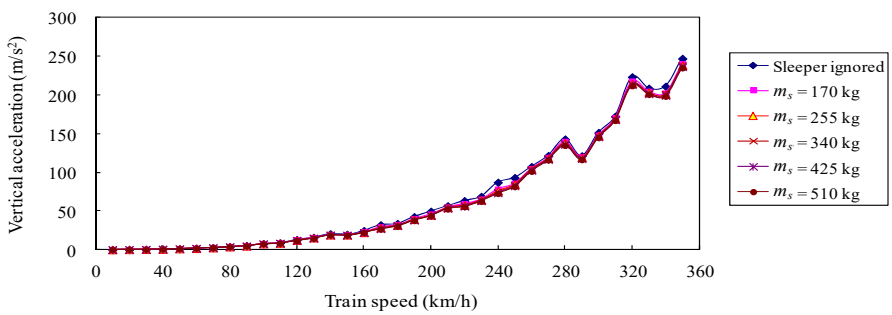

Figure 31: Maximum vertical acceleration of rail with respect to train speed.

5.4 Example 3: Influence of Two Types of Wheel–Rail Interaction Models on Dynamic Responses of TTBI System

In this example, two types of wheel-rail interaction models are considered, i.e., the no-jump model and the jump model. The same train, track, bridge, and track irregularity as that presented in Section 5.1 is used, with LBE = 5.0 m and LRE = 0.625 m. The wheels of each vehicle are considered to be in full contact with the rails at all times for the no-jump model (Yang et al., 2004, Lou and Zeng, 2005), while the wheels are free to jump from the rails for the jump model (Zhai and Sun, 1994).

The running safety of trains has been of great concern in railway engineering for a long time, particularly in relation to the development of high-speed railways and the need to upgrade existing railways. Several mechanisms that can result in the derailment of a running train have been identified through analytical and experimental investigations, and a number of indices have been proposed based on these to evaluate the possibility, or risk, of train derailment. One of these indices is the offload factor, *PD*, (Yang et al., 2004). Large *PD* values indicate that dynamic vertical wheel–rail force acting on the wheel is substantially reduced. This is detrimental to the lateral stability of the wheelset, and thus a limit needs to be placed on the value of the *PD* index to prevent the wheelset from derailing. An upper limit of 0.60 on the *PD* value was used in Chinese specifications for the design of railways (Xia et al., 2006), which implies that jumps between the vehicle's wheels and the rails are not usually permitted in practice. Therefore, the wheels of a vehicle are generally assumed to be in constant contact with the rails (i.e., the no-jump model) when most train–track–bridge interaction problems occur. Based on this assumption, the dynamic contact forces between the wheels and rails are considered as internal forces, and it is thus not necessary to calculate the internal forces when setting up the equations of motion of a TTBI system (Lou and Zeng, 2005). As such, the vehicle response, wheel–rail contact force, track response, and bridge response can be computed with no iterations required. However, in some extreme cases, such as with poor track quality or during an earthquake, the wheels may jump upward and separate from the rails (i.e., the jump model) and the train then has a high risk of derailment. When studying the dynamic responses of a TTBI system using the jump model, two sets of equations of motion can be written, one for the moving train subsystem and the other for the track–bridge subsystem. These equations are coupled with the wheel–rail contact forces existing at the contact points of the two subsystems, and are usually solved using procedures of an iterative nature (Zhai and Sun, 1994). For instance, when first assuming a trial solution for the wheel–rail contact forces, the dynamic responses of the train and track–bridge subsystems can be solved from the two sets of equations of motion, respectively. An improved solution for the wheel–rail contact forces can then be obtained according to the displacements of the wheels and rails at the contact points. By substituting these forces into the equations of motion within a train and track–bridge subsystems, an improved solution for the dynamic responses of the two subsystems can be solved. However, to avoid divergence and improve the convergence rate of iteration, sufficiently small time steps are required in the process of calculation, which may thus result in more computer time.

Seven cases with train speeds of 50 km/h, 100 km/h, 150 km/h, 200 km/h, 250 km/h, 300 km/h, and 350 km/h are considered. The dynamic responses of the TTBI system obtained using the no-jump and jump wheel–rail interaction models at various train speeds are shown in Table 6. As is evident from the table, the solutions obtained using the no-jump model for the seven cases given

agree very well with those of the jump model, although the impact response induced by the jump model appears to increase slightly. The differences in bridge acceleration are no larger than 2.00%, due to the relatively larger stiffness and mass of the bridge. However, although the differences in the dynamic responses of the sleeper, rail, and vehicle are slightly larger, all of them are smaller than 5.00%. It should be noted that the total CPU times for the no-jump model and the jump model at a train speed of 350 km/h are 902.4 s and 7183.1 s on a 2.8 GHz personal computer, respectively, and the ratio of the former to the latter is 0.126. Therefore, it is concluded that the no-jump wheel-rail interaction model can be reliably and efficiently used to predict the spatial dynamic responses of a TTBI system.

Train speed (km/h)		50	100	150	200	250	300	350
Bridge midpoint lateral acceleration (m/s^2)	no-jump model	0.005	0.015	0.023	0.052	0.068	0.106	0.152
	jump model	0.005	0.015	0.023	0.053	0.069	0.107	0.153
Bridge midpoint vertical acceleration (m/s^2)	no-jump model	0.008	0.036	0.100	0.151	0.253	0.403	0.610
	jump model	0.008	0.036	0.101	0.154	0.257	0.411	0.618
Sleeper lateral acceleration (m/s^2)	no-jump model	0.096	0.743	2.378	6.209	10.047	14.180	18.651
	jump model	0.099	0.758	2.432	6.347	10.165	14.459	18.757
Sleeper vertical acceleration (m/s^2)	no-jump model	0.194	0.909	3.005	6.865	10.822	20.809	39.986
	jump model	0.200	0.910	3.038	6.878	10.864	21.494	41.097
Rail lateral acceleration (m/s^2)	no-jump model	0.557	2.436	5.917	12.511	21.175	36.174	49.852
	jump model	0.564	2.528	5.925	12.730	21.498	37.281	51.437
Rail vertical acceleration (m/s^2)	no-jump model	1.151	7.542	18.837	44.083	83.549	148.46	238.90
	jump model	1.162	7.726	19.256	45.507	86.512	154.062	242.197
Carbody lateral acceleration (m/s^2)	no-jump model	0.059	0.133	0.172	0.179	0.188	0.237	0.296
	jump model	0.060	0.134	0.173	0.179	0.190	0.241	0.298
Carbody vertical acceleration (m/s^2)	no-jump model	0.103	0.150	0.237	0.320	0.368	0.462	0.531
	jump model	0.105	0.151	0.242	0.322	0.373	0.471	0.545
Bogie lateral acceleration (m/s^2)	no-jump model	0.663	2.136	4.341	6.170	6.339	7.210	7.946
	jump model	0.678	2.165	4.356	6.193	6.379	7.361	7.996
Bogie vertical acceleration (m/s^2)	no-jump model	0.558	1.599	3.434	5.444	8.510	13.558	18.209
	jump model	0.576	1.614	3.561	5.520	8.576	13.694	18.657
Lateral force of fastener (kN)	no-jump model	0.634	1.638	3.059	4.026	4.932	5.242	5.733
	jump model	0.643	1.655	3.135	4.096	5.013	5.386	5.782
Vertical pressure of fastener (kN)	no-jump model	28.543	29.600	31.462	33.908	37.420	41.791	47.013
	jump model	29.407	30.492	31.940	34.678	37.533	41.881	48.01
Derailment factor	no-jump model	0.047	0.092	0.138	0.166	0.227	0.304	0.471
	jump model	0.048	0.092	0.140	0.168	0.227	0.306	0.473
Offload factor	no-jump model	0.038	0.073	0.128	0.222	0.337	0.454	0.591
	jump model	0.039	0.074	0.129	0.228	0.341	0.467	0.603

Table 6: Calculation results for two wheel–rail interaction models at various train speeds.

6 SUMMARY AND OUTLOOK

Based on obvious differences in the flexural rigidity between the rail and bridge, a 3D rail–bridge coupling element of unequal lengths is presented. The spatial dynamic responses of a TTBI system with a seven-span continuous beam bridge are studied using a 3D rail–bridge coupling element of unequal lengths and equal lengths. Furthermore, the effects of two types of track models on the spatial dynamic responses of the TTBI system are investigated, and the following conclusions can be drawn from the numerical results.

(1) The proposed 3D rail–bridge coupling element with shorter rail elements and longer bridge elements not only helps save calculation time, but it also delivers satisfactory results when investigating the spatial dynamic responses of a TTBI system.

(2) In analyzing the spatial dynamic responses of a TTBI system using a 3D rail–bridge coupling element that has the same length as the bridge element, the influence of the length of the rail element is significant, not only on the rail dynamic responses but also on the bridge dynamic responses, when the track irregularities are considered. This differs from the case with an ideal smooth track.

(3) There are differences in the dynamic responses based on the single-layer and double-layer track models, and the differences in both the maximum lateral and vertical dynamic responses generally increase with an increase in the mass of the sleeper and the train speed, particularly with respect to accelerations of the bridge and rail. In addition, the two-layer track model is more accurate.

(4) The no-jump assumption between the vehicle's wheels and the rails can be reliably and efficiently used for most train–track–bridge interaction problems.

(5) Further studies on the efficiency and accuracy of the proposed 3D rail–bridge coupling element are needed to investigate the spatial dynamic responses of a TTBI system during an earthquake, due to the fact that vibrations of the system may be more violent during such an occurrence.

Acknowledgments

The research work described in this paper was supported by the Joint Fund of the National Natural Science Foundation of China (Grant Nos. U1361204, U1334203, and U1434204); the Project of Innovation-driven Plan in Central South University (Grant No. 2015CXS014); the Fundamental Research Funds for the Central Universities of Central South University (No. 2016zzts067).

References

Ayre R.S., Ford G., Jacobsen L.S., (1950). Transverse vibration of a two-span beam under action of a moving constant force. Journal of Applied Mechanics 17(1): 1–12.

Chatterjee P.K., Datta T.K., Surana C.S., (1994). Vibration of suspension bridges under vehicular movement. Journal of Structural Engineering, ASCE 120(3): 681–703.

Cheng Y.S., Au F.T.K., Bowe C., O'Dwyer D., (2001). Vibration of railway bridges under a moving train by using bridge–track–vehicle element. Engineering Structures 23(12): 1597–1606.

Chu K.H., Garg V.K., Wang T.L., (1979). Railway–bridge impact: Simplified train and bridge model. Journal of the Structural Division, ASCE 105(9): 1823–1844.

Dinh V.N., Kim K.D., Warnitcha P., (2009). Dynamic analysis of three-dimensional bridge–high-speed train interactions using a wheel–rail contact model. Engineering Structures 31(12): 3090–3106.

Frýba L., (1972). Vibration of solids and structures under moving loads. The Netherlands: Noordhoff International Publishing.

Ichikawa M., Miyakawa Y., Matsuda A., (2000). Vibration analysis of the continuous beam subjected to a moving mass. Journal of Sound and Vibration 230(3): 493–506.

Kalker J.J., (1967). On the rolling contact of two elastic bodies in the response of dry friction. The Netherlands: Delft University of Technology.

Kim S., (2011). Experimental evaluations of track structure effects on dynamic properties of railway bridges. Journal of Vibration and Control 17(12): 1817–1826.

Kwasniewski L., Li H., Wekezer J., Malachowski J., (2006). Finite element analysis of vehicle–bridge interaction. Finite Elements in Analysis and Design 42(11): 950–959.

Lei X., Noda N.A., (2002). Analyses of dynamic response of vehicle and track coupling system with random irregularity of track vertical profile. Journal of Sound and Vibration 258(1): 147–165.

Lei X.Y., Wang J., (2014). Dynamic analysis of the train and slab track coupling system with finite elements in a moving frame of reference. Journal of Vibration and Control 20(9): 1301–1317.

Lei X.Y., Zhang B., (2011). Analyses of dynamic behavior of track transition with finite elements. Journal of Vibration and Control 17(11): 1733–1747.

Liu K., Reynders K., De Roeck G., Lombaert G., (2009). Experimental and numerical analysis of a composite bridge for high-speed trains. Journal of Sound and Vibration 320(1–2): 201–220.

Lou P. (2007). Finite element analysis for train–track–bridge interaction system. Archive of Applied Mechanics 77(10): 707–728.

Lou P., (2005). A vehicle–track–bridge interaction element considering vehicle's pitching effect. Finite Elements in Analysis and Design 41(4): 397–427.

Lou P., and Zeng Q.Y., (2005). Formulation of equations of motion of finite element form for vehicle–track–bridge interaction system with two types of vehicle model. International Journal for Numerical Methods in Engineering 62(3): 435–474.

Lou P., Yu Z.W., Au F.T.K., (2012). Rail–bridge coupling element of unequal lengths for analysing train–track–bridge interaction systems. Applied Mathematical Modelling 36(4): 1395–1414.

Lu F., Lin J.H., Kennedy D. and Williams F.W., (2009). An algorithm to study non-stationary random vibrations of vehicle-bridge systems. Computers and Structures 87(3–4): 177–185.

Nguyen D.V., Kim K.D., Warnitchai P., (2009). Dynamic analysis of three-dimensional bridge–high-speed train interactions using a wheel–rail contact model. Engineering Structures 31(12): 3090–3106.

Song M.K., Noh H.C., Choi C.K., (2003). A new three-dimensional finite element analysis model of high-speed train–bridge interactions. Engineering Structures 25(13): 1611–1626.

Sun Y.Q., Dhanasekar M., (2002). A dynamic model for the vertical interaction of the rail track and wagon system. International Journal of Solid and Structures 39(5): 1337–1359.

Wang Y.J., Wei Q.C., Shi J., Long X.Y., (2010). Resonance characteristics of two-span continuous beam under moving high speed trains. Latin American Journal of Solids and Structures 7(2): 185-199.

Wu J.S., Dai C.W., (1987). Dynamic responses of multispan nonuniform beam due to moving loads. Journal of Structural Engineering, ASCE 113(3): 458–474.

Wu Y.S., and Yang Y.B., (2003). Steady-state response and riding comfort of trains moving over a series of simply supported bridges. Engineering Structures 25(2): 251–265.

Wu Y.S., Yang Y.B., and Yau J.D., (2001). Three-dimensional analysis of train–rail–bridge interaction problems. Vehicle System Dynamics 36(1): 1–35.

Xia H., Han Y., Zhang N., Guo W.W., (2006). Dynamic analysis of train–bridge system subjected to non-uniform seismic excitations. Earthquake Engineering and Structural Dynamics 35: 1563–1579.

Xia H., Xu Y.L., Chan T.H.T., (2000). Dynamic interaction of long suspension bridges with running trains. Journal of Sound and Vibration 237(2): 263–280.

Xin T., Gao L., (2011). Reducing slab track vibration into bridge using elastic materials in high speed railway. Journal of Sound and Vibration 330(10): 2237–2248.

Xu Q.Y., Yan B., Lou P., Zhou X.L., (2015). Influence of slab length on dynamic characteristics of subway train-steel spring floating slab track-tunnel coupled system. Latin American Journal of Solids and Structures 12(4): 649-674.

Yang Y.B., Chang C.H., Yau J.D., (1999). An element for analyzing vehicle–bridge systems considering vehicle's pitching effect. International Journal for Numerical Methods in Engineering 46(7): 1031–1047.

Yang Y.B., Yau J.D., Wu Y.S., (2004). Vehicle–bridge interaction dynamics: with applications to high-speed railways. Singapore: World Scientific.

Zakeri J.A., Shadfar M., Feizi M.M., (2014). Sensitivity analysis of bridge-track-train system to parameters of railway. Latin American Journal of Solids and Structures 11(4): 598-612.

Zeng Q.Y., (2000). The principle of a stationary value of total potential energy of dynamic system. Journal of Huazhong University of Science and Technology 28(1): 1–3.

Zhai W.M., Cai C.B., and Guo S.Z., (1996). Coupled model of vertical and lateral vehicle/track interactions. Vehicle System Dynamics 26(1): 61–79.

Zhai W.M., Sun X., (1994). A detailed model for investigating vertical interaction between railway vehicle and Track. Vehicle System Dynamics 23(Suppl): 603–615.

Zhai W.M., Xia H., (2011). Train–track–bridge dynamic interaction theory and engineering application. Beijing: Science Press.

Zhai W.M., Xia H., Cai C.B., Gao M.M., Li X.Z., Guo X.R., Zhang N., Wang K.Y., (2013) .High-speed train–track–bridge dynamic interactions-Part I: theoretical model and numerical simulation. International Journal of Rail Transportation 1(1–2): 3–24.

Zhang N., Xia H., De Roeck G., (2010). Dynamic analysis of train–bridge system under multi-support seismic excitations. Journal of Mechanical Science and Technology 24(11): 2181–2188.

Zhang N., Xia H., Guo W.W., Zhan J.W., Yao J.B., Gao Y.M., (2010). Vehicle–bridge interaction analysis of heavy load railway. Procedia Engineering 4: 347–354.